Theoretical framework of entangled-photon generation from biexcitons in nano-to-bulk crossover regime with planar geometry

Motoaki Bamba[1, *] and Hajime Ishihara[2]

[1]*Department of Materials Engineering Science, Osaka University, Toyonaka, Osaka 560-8531, Japan*
[2]*Department of Physics and Electronics, Osaka Prefecture University, Sakai, Osaka 599-8531, Japan*
(Dated: May 16, 2011)

We have constructed a theoretical framework of the biexciton-resonant hyperparametric scattering for the pursuit of high-power and high-quality generation of entangled photon pairs. Our framework is applicable to nano-to-bulk crossover regime where the center-of-mass motion of excitons and biexcitons is confined. Material surroundings and the polarization correlation of generated photons can be considered. We have analyzed the entangled-photon generation from CuCl film, by which ultraviolet entangled-photon pairs are generated, and from dielectric microcavity embedding a CuCl layer. We have revealed that in the nano-to-bulk crossover regime we generally get a high performance from the viewpoint of statistical accuracy, and the generation efficiency can be enhanced by the optical cavity with maintaining the high performance. The nano-to-bulk crossover regime has a variety of degrees of freedom to tune the entangled-photon generation, and the scattering spectra explicitly reflect quantized exciton-photon coupled modes in the finite structure.

PACS numbers: 42.65.Lm, 42.50.Nn, 71.35.-y, 71.36.+c

I. INTRODUCTION

Entangled photon pairs have been discussed in relation with the Einstein-Padolsky-Rosen (EPR) paradox,[1] and nowadays they play an important role in quantum information technologies. The pursuit of their high-quality and high-efficiency generation is a fascinating subject in the fields of quantum optics and solid-state physics. In addition to the standard generation method by parametric down-conversion (PDC) in second-order nonlinear crystals[2,3] the generation scheme using a semiconductor quantum dot[4–8] attracts much attention, because purely a single pair of entangled photons is created in principle, and it can be a deterministic source of entangled pairs. Recently, the generation efficiency is highly enhanced by implementing an optical cavity structure with distributed Bragg reflectors (DBRs)[6] and by a molecule of micropillars.[8] Further, the emission by electric injection has been reported.[7] On the other hand, the development of entangled photons as an excitation light source is of growing importance for the next-generation technologies of fabrication and chemical reaction.[9] For this purpose, high-power and high-quality entangled-photon beams are absolutely necessary, and this high-power but probabilistic generation is another direction of research in addition to the deterministic generation by single quantum dots.

In the process of PDC,[2,3] an incident photon with frequency $\omega_{\rm in}$ and wavenumber $\boldsymbol{k}_{\rm in}$ splits into two photons $(\omega_1, \boldsymbol{k}_1)$ and $(\omega_2, \boldsymbol{k}_2)$ with satisfying the conservation of energy $\omega_{\rm in} = \omega_1 + \omega_2$ and of wavevector $\boldsymbol{k}_{\rm in} = \boldsymbol{k}_1 + \boldsymbol{k}_2$. This second-order nonlinear process creates polarization-correlated entangled-photon pairs in nonlinear optical crystals with a birefringence. On the other hand, Savasta et al.[12] suggested and Edamatsu et al.[10] experimentally demonstrated that ultraviolet entangled-photon pairs are generated by the biexciton-resonant hy-
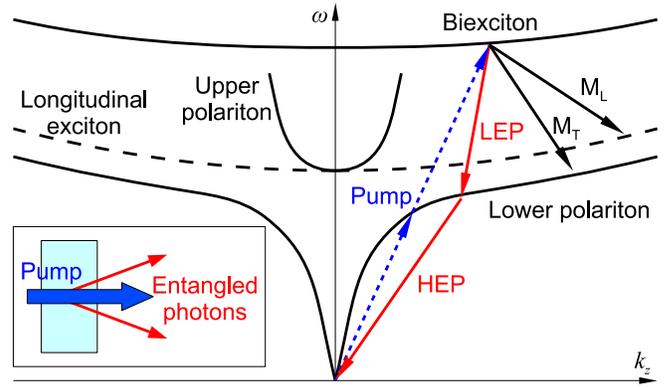

FIG. 1: The biexciton-resonant hyperparametric scattering (RHPS) is depicted on dispersion curves of biexciton, exciton-polariton, and longitudinal exciton. Biexcitons are resonantly created by two-photon absorption, and entangled-photon pairs are emitted when the biexcitons decay into the lower exciton-polariton branch. This emission appears in scattering spectrum as two peaks called LEP and HEP (lower and higher energy polaritons) as seen in Fig. 3. Due to the conservation of energy and wavevector, the positions of the two peaks depend on scattering angle,[10,11] and the entangled two photons are emitted symmetrical about the pump beam as shown in the inset. Two additional peaks called $\rm M_T$ and $\rm M_L$ in scattering spectra originate from the biexciton decay into transverse and longitudinal exciton levels, respectively.

perparametric scattering (RHPS) in CuCl (see Fig. 1). The RHPS is a third-order nonlinear process, in which two incident photons resonantly creates a biexciton (excitonic molecule) with $(2\omega_{\rm in}, 2\boldsymbol{k}_{\rm in})$ and it spontaneously collapses into a photon pair satisfying $2\omega_{\rm in} = \omega_1 + \omega_2$ and $2\boldsymbol{k}_{\rm in} = \boldsymbol{k}_1 + \boldsymbol{k}_2$. Since the lowest level of biexcitons in CuCl, which was resonantly excited in the experiment, has zero angular momentum,[11] the emitted pair consists

of left- and right-circularly polarized photons conserving the total angular momentum. Owing to the two possible decay paths involving exciton-polaritons, the emitted photons are polarization-entangled.

The generation efficiency of RHPS is much higher than that of PDC, because of the giant oscillator strength of the two-photon absorption involving the biexciton.[11] However, in the first experiment,[10] a part of observed pairs has no entanglement, and this noise was subtracted in the estimation of entanglement of the generated pairs. As indicated by Oohata et al.,[13] the main contribution of the unentangled pairs is an accidental collapse of two biexcitons, and this problem has been successfully suppressed by using high-repetition and weak-power laser pulses, because the number of unentangled pairs (noise) is increased by I_{in}^4 for increasing the pumping power I_{in} while the number of entangled pairs (signal) is proportional to I_{in}^2. However, this fundamental trade-off problem between signal intensity and S/N ratio should be resolved from the improvement of material structures[14] in addition to the improvement of pumping condition of Ref. 13. While one solution is using a single quantum dot as a deterministic source,[4–8] for the pursuit of high-power generation there is a proposal of using an optical cavity embedding an excitonic quantum well for the improvement of generation efficiency.[15,16] Furthermore, owing to the rapid radiative decay by the exciton superradiance (enhancement of interaction volume between excitons and photons),[17,18] we have theoretically revealed that the trade-off problem can be resolved simultaneously realizing a high generation efficiency by using an optical cavity embedding an excitonic layer in nano-to-bulk crossover regime.[14]

In a microcrystal, such as quantum dot and quantum well, smaller than the Bohr radius of excitons, the electron and hole are individually confined in the crystal, and the relative motion of excitons and also the binding energy are strongly modified from those in bulk crystal. When the crystal size is larger than the exciton Bohr radius but small enough compared to the light wavelength, the center-of-mass motion of excitons are confined, and the center-of-mass kinetic energy is quantized.[19,20] When the crystal size is comparable or a few times larger than the wavelength (nano-to-bulk crossover regime), the system is characterized by exciton-photon coupled modes with peculiar resonance energy and radiative life time, and the coupled modes are gradually reduced to bulk polaritons with increasing the crystal size.[18,21–25] In this crossover regime, the system shows a variety of optical responses compared to bulk materials and also to quantum dots due to the center-of-mass confinement of excitons and the spatially resonant coupling with electromagnetic fields. Actually, owing to the recent development of nanoscale fabrication, anomalous nonlinear optical processes have been reported in semiconductor nano-structures and in the nano-to-bulk crossover regime.[17,26–36] Further, it shows a rapid radiative decay rate of excitons on the order of 100 fs due to the exciton superradiance.[17] Con-

cerning the entangled photon generation, while the performance of PDC method is almost governed by the choice of nonlinear materials and its thickness, the RHPS method significantly depends on the quantum states of excitons and biexcitons, because it is a resonant process involving the elementary excitations. In the nano-to-bulk crossover regime, the generation of entangled photon pairs by RHPS can be significantly modified with respect to frequencies, angles, polarizations, and phase difference of the generated entangled state as discussed in our previous letter.[14] In the present long paper, we will show the detailed theoretical framework for the investigation of the entangled-photon generation in nano-to-bulk crossover regime with multilayer structures, especially an excitonic layer embedded in DBRs.

We explain our theoretical framework in Sec. II, and show in detail the way to calculate the one-photon scattering intensity and the two-photon coincidence intensity of RHPS in the case of multilayer structure in Sec. III. The calculation results are shown in Sec. IV, and the discussion is summarized in Sec. V.

II. THEORETICAL FRAMEWORK

The emission spectra from Bose-Einstein condensation of biexcitons were calculated by Inoue and Hanamura,[37] and they also showed the relation between energies and scattering angles of two peaks called LEP and HEP (lower and higher energy polaritons). Later, Hanamura and Takagahara[38] calculated line shapes of the so-called M_T and M_L peaks, which are emitted by the relaxations of biexcitons to transverse and longitudinal excitons, respectively. The entanglement of the scattered photons by RHPS was first pointed out by Savasta et al.,[12] and their theoretical framework[39] is based on the quantum electrodynamics (QED) theory for dispersive and absorbing media[40,41] and on the exciton-exciton correlation functions calculated from first principles.[42,43]

In the present paper, in order to correctly treat the center-of-mass confinement of excitons, we start from the QED theory of excitons,[44] which simultaneously solves the equation of motion of excitons and of electromagnetic fields with inheriting the concepts of the above QED theories[40,41] and of the semiclassical nonlocal theory[30,45] (or the so-called ABC-free theory[46]). It is well known that the center-of-mass motion of excitons raises more than one propagating modes of exciton-polaritons in their band gap frequency, and the RHPS process has been used to observe the dispersion of polaritons[11,37,47–49] and also to measure the translational masses of excitons and biexcitons.[11,50–52] Moreover, optical responses explicitly reflects the confinement of center-of-mass motion of excitons in nano-structured materials and also in the nano-to-bulk crossover regime,[17–20,26–36] which we investigate in the present paper.

Concerning the treatment of biexcitons, we suppose the excitons as pure bosons and consider an exciton-

exciton interaction leading to the creation of biexcitons. However, instead of the detailed treatment in the theory of Savasta et al.,[39] we simply assume the relative motion of the lowest level of biexcitons with some parameters measured in experiments,[11,53,54] and the coefficients of the exciton-exciton interaction is replaced by the wavefunction and the binding energy of biexcitons. This treatment is very simple and useful to catch the behavior of biexciton lowest level in CuCl even in the nano-to-bulk crossover regime, because the exciton and biexciton states in CuCl has been well analyzed by the bipolariton theory[55,56] and RHPS experiments.[54,57,58] While the treatment of biexcitons is in general a four-body problem with two electrons and two holes and it is usually a hard work, owing to the above mentioned simple treatment, we can easily discuss the polarization correlation of photon pairs emitted from the biexciton lowest level, which has no angular momentum.

Moreover, by the use of the dyadic Green's function for the wave equation of electric field, we can consider the surroundings of excitonic material, such as an optical cavity consisting of two DBRs. In order to extract the scattering fields, instead of using the input-output relation,[41,59–63] we consider the definition of Green's function and commutation relations of fluctuation operators. This simple treatment is valid at least in multilayer systems and useful to consider complicated structures.

In the following subsections, we show our theoretical framework to calculate the signal and noise intensities by RHPS. We show the Hamiltonian in Sec. II A, and the equations of motion are derived in Sec. II B. In order to discuss the RHPS, we use some approximations, which are explained in Sec. II C. The model of biexcitons are shown in Sec. II D. In order to solve the equations of motion, we use the Green's function technique explained in Sec. II E. Finally, we derive the expression of observables in Sec. II F.

A. Hamiltonian

Our theoretical framework is based on the QED theory of excitons.[44] The Hamiltonian is written as

$$\hat{H} = \hat{H}_{\text{ex}} + \hat{H}_{\text{res}} + \hat{H}_{\text{int}} + \hat{H}_{\text{em}}, \tag{1}$$

where $\hat{H}_{\text{ex}}$ describes the excitonic system, $\hat{H}_{\text{res}}$ represents a reservoir for the nonradiative damping of excitons, $\hat{H}_{\text{int}}$ is the exciton-photon interaction, and $\hat{H}_{\text{em}}$ describes the electromagnetic fields and a background dielectric medium as discussed in Ref. 64 and also used in Ref. 44. In order to discuss the biexciton-associated RHPS, we consider an exciton-exciton interaction with coefficient $V_{\mu,\nu;\mu',\nu'}$. Namely, the Hamiltonian of excitonic system is written as

$$\hat{H}_{\text{ex}} = \sum_{\mu} \hbar\omega_{\mu}\hat{b}_{\mu}^{\dagger}\hat{b}_{\mu} + \frac{1}{2}\sum_{\mu,\mu',\nu,\nu'} V_{\mu,\nu;\mu',\nu'}\hat{b}_{\mu}^{\dagger}\hat{b}_{\nu}^{\dagger}\hat{b}_{\nu'}\hat{b}_{\mu'}, \tag{2}$$

where $\hat{b}_{\mu}$ is the annihilation operator of an exciton in state μ and ω_{μ} is its eigenfrequency. We treat the excitons as pure bosons satisfying

$$\left[\hat{b}_{\mu}, \hat{b}_{\mu'}^{\dagger}\right] = \delta_{\mu,\mu'}, \tag{3a}$$

$$\left[\hat{b}_{\mu}, \hat{b}_{\mu'}\right] = 0, \tag{3b}$$

and their non-bosonic behavior is described by the exciton-exciton interaction, the second term in Eq. (2). The reservoir $\hat{H}_{\text{res}}$ is written as

$$\hat{H}_{\text{res}} = \sum_{\mu} \int_{0}^{\infty} \mathrm{d}\Omega \left\{ \hbar\Omega\hat{d}_{\mu}^{\dagger}(\Omega)\hat{d}_{\mu}(\Omega) \right.$$
$$\left. + \left[\hat{b}_{\mu} + \hat{b}_{\mu}^{\dagger}\right]\left[g_{\mu}(\Omega)\hat{d}_{\mu}(\Omega) + g_{\mu}^{*}(\Omega)\hat{d}_{\mu}^{\dagger}(\Omega)\right] \right\}, \tag{4}$$

where $\hat{d}_{\mu}(\Omega)$ is the annihilation operator of harmonic oscillator with frequency Ω interacting with excitons in state μ, and $g_{\mu}(\Omega)$ is the coupling coefficient. The oscillators are independent with each other and satisfy the following commutation relations:

$$[\hat{d}_{\mu}(\Omega), \hat{d}_{\mu'}^{\dagger}(\Omega')] = \delta_{\mu,\mu'}\delta(\Omega - \Omega'), \tag{5a}$$

$$[\hat{d}_{\mu}(\Omega), \hat{d}_{\mu'}(\Omega')] = 0. \tag{5b}$$

Further, $\hat{H}_{\text{int}}$ is simply written as a product of electric field $\hat{\boldsymbol{E}}(\boldsymbol{r})$ and excitonic polarization $\hat{\boldsymbol{P}}_{\text{ex}}(\boldsymbol{r})$:

$$\hat{H}_{\text{int}} = -\int \mathrm{d}\boldsymbol{r} \ \hat{\boldsymbol{P}}_{\text{ex}}(\boldsymbol{r}) \cdot \hat{\boldsymbol{E}}(\boldsymbol{r}). \tag{6}$$

Here, the excitonic polarization is represented as

$$\hat{\boldsymbol{P}}_{\text{ex}}(\boldsymbol{r}) = \sum_{\mu} \boldsymbol{\mathcal{P}}_{\mu}(\boldsymbol{r})\hat{b}_{\mu} + \text{H.c.}, \tag{7}$$

where the coefficient $\boldsymbol{\mathcal{P}}_{\mu}(\boldsymbol{r})$ is expressed by the exciton center-of-mass wavefunction $g_{\mu}^{\text{ex}}(\boldsymbol{r})$ and unit vector $\boldsymbol{e}_{\mu}$ of polarization direction as

$$\boldsymbol{\mathcal{P}}_{\mu}(\boldsymbol{r}) = M\boldsymbol{e}_{\mu}g_{\mu}^{\text{ex}}(\boldsymbol{r}). \tag{8}$$

The absolute value of M can be evaluated by the longitudinal-transverse (LT) splitting energy $\Delta_{\text{LT}} = |M|^{2}/\varepsilon_{0}\varepsilon_{\text{bg}}^{\text{ex}}$ of excitons, the vacuum permittivity ε_{0}, and the background dielectric constant $\varepsilon_{\text{bg}}^{\text{ex}}$ of the excitonic medium.

B. Equations of motion

According to Ref. 44 or the QED theories of dispersive and absorbing media,[40,41,64] the equation of motion of electric field $\hat{\boldsymbol{E}}(\boldsymbol{r})$ is derived in frequency domain as

$$\boldsymbol{\nabla} \times \boldsymbol{\nabla} \times \check{\boldsymbol{E}}^{+}(\boldsymbol{r},\omega) - \frac{\omega^{2}}{c^{2}}\varepsilon_{\text{bg}}(\boldsymbol{r},\omega)\check{\boldsymbol{E}}^{+}(\boldsymbol{r},\omega)$$
$$= \mathrm{i}\mu_{0}\omega\check{\boldsymbol{J}}_{0}(\boldsymbol{r},\omega) + \mu_{0}\omega^{2}\check{\boldsymbol{P}}_{\text{ex}}^{+}(\boldsymbol{r},\omega). \tag{9}$$

Here, μ_0 is the vacuum permeability, $\varepsilon_{\mathrm{bg}}(\boldsymbol{r},\omega)$ is the dielectric function of the background medium with arbitrary three dimensional structure. We write an operator with a check ($\check{\ }$) in frequency domain. $\check{\boldsymbol{J}}_0(\boldsymbol{r},\omega)$ describes the fluctuation of electromagnetic fields and satisfies

$$\left[\check{\boldsymbol{J}}_0(\boldsymbol{r},\omega),\{\check{\boldsymbol{J}}_0(\boldsymbol{r}',\omega'^*)\}^\dagger\right]=\left[\check{\boldsymbol{J}}_0(\boldsymbol{r},\omega),\check{\boldsymbol{J}}_0(\boldsymbol{r}',-\omega')\right]$$
$$=\delta(\omega-\omega')\delta(\boldsymbol{r}-\boldsymbol{r}')\frac{\varepsilon_0\hbar\omega^2}{\pi}\mathrm{Im}[\varepsilon_{\mathrm{bg}}(\boldsymbol{r},\omega)]\overleftrightarrow{\boldsymbol{1}}. \quad (10)$$

In the same manner as in Ref. 44, we obtain the equation of excitons' motion in frequency domain as

$$[\hbar\omega_\mu-\hbar\omega-\mathrm{i}\gamma_{\mathrm{ex}}/2]\,\check{b}_\mu(\omega)$$
$$=\int\mathrm{d}\boldsymbol{r}\,\boldsymbol{\mathcal{P}}_\mu^*(\boldsymbol{r})\cdot\check{\boldsymbol{E}}^+(\boldsymbol{r},\omega)+\check{\mathcal{D}}_\mu(\omega)$$
$$-\sum_\nu\sum_{\mu',\nu'}V_{\mu,\nu;\mu',\nu'}\int_{-\infty}^\infty\mathrm{dt}\,\frac{\mathrm{e}^{\mathrm{i}\omega t}}{2\pi}\hat{b}_\nu^\dagger(t)\hat{b}_{\nu'}(t)\hat{b}_{\mu'}(t), \quad (11)$$

where γ_{ex} is the nonradiative damping width defined in terms of $\{g_\mu(\Omega)\}$ as shown in Eq. (D7) of Ref. 44, and $\check{\mathcal{D}}_\mu(\omega)$ represents the fluctuation by the damping satisfying

$$\left[\check{\mathcal{D}}_\mu(\omega),\{\check{\mathcal{D}}_{\mu'}(\omega'^*)\}^\dagger\right]=\left[\check{\mathcal{D}}_\mu(\omega),\check{\mathcal{D}}_{\mu'}(-\omega')\right]$$
$$=\delta_{\mu,\mu'}\delta(\omega-\omega')\frac{\hbar\gamma_{\mathrm{ex}}}{2\pi}. \quad (12)$$

The last term on the right hand side of Eq. (11) is the nonlinear term due to the exciton-exciton interaction.

Here, we define a new operator

$$\hat{B}_\lambda\equiv\frac{1}{2}\sum_{\mu,\nu}F_{\lambda,\mu,\nu}^*\hat{b}_\nu\hat{b}_\mu, \quad (13)$$

which annihilates a biexciton (excitonic molecule) in state λ and describes a two-exciton eigen state $\hat{B}_\lambda^\dagger|\mathrm{g}\rangle$ by applying it to the ground state $|\mathrm{g}\rangle$ of matter system. The coefficient $F_{\lambda,\mu,\nu}$ is invariant by the exchange of two exciton indices as

$$F_{\lambda,\mu,\nu}=F_{\lambda,\nu,\mu}. \quad (14)$$

Further, it is ortho-normal

$$\frac{1}{2}\sum_{\mu,\nu}F_{\lambda,\mu,\nu}F_{\lambda',\mu,\nu}^*=\delta_{\lambda,\lambda'}, \quad (15)$$

and also has a completeness

$$\sum_\lambda F_{\lambda,\mu,\nu}F_{\lambda,\mu',\nu'}^*=\delta_{\mu,\mu'}\delta_{\nu,\nu'}+\delta_{\mu,\nu'}\delta_{\nu,\mu'}. \quad (16)$$

From the excitonic Hamiltonian $\hat{H}_{\mathrm{ex}}$ [Eq. (2)], the coefficient $F_{\lambda,\mu,\nu}$ and eigen frequency Ω_λ of biexciton eigen state λ should satisfy

$$(\hbar\omega_\mu+\hbar\omega_\nu)F_{\lambda,\mu,\nu}+\sum_{\mu',\nu'}V_{\mu,\nu;\mu',\nu'}F_{\lambda,\mu',\nu'}=\hbar\Omega_\lambda F_{\lambda,\mu,\nu}. \quad (17)$$

By using Eqs. (14) and (16), we can rewrite Eq. (13) as

$$\sum_\lambda F_{\lambda,\mu,\nu}\hat{B}_\lambda=\hat{b}_\nu\hat{b}_\mu. \quad (18)$$

Therefore, from this relation and Eq. (17), we can rewrite Eq. (11) as

$$[\hbar\omega_\mu-\hbar\omega-\mathrm{i}\gamma_{\mathrm{ex}}/2]\,\check{b}_\mu(\omega)=\int\mathrm{d}\boldsymbol{r}\,\boldsymbol{\mathcal{P}}_\mu^*(\boldsymbol{r})\cdot\check{\boldsymbol{E}}^+(\boldsymbol{r},\omega)+\check{\mathcal{D}}_\mu(\omega)$$
$$+\sum_{\lambda,\nu}(\hbar\omega_\mu+\hbar\omega_\nu-\hbar\Omega_\lambda)F_{\lambda,\mu,\nu}\int_{-\infty}^\infty\mathrm{d}\omega'\,\{\check{b}_\nu(\omega'-\omega)\}^\dagger\check{B}_\lambda(\omega'). \quad (19)$$

On the other hand, by deriving the equation of motion for $\hat{B}_\lambda$ and by using the above relations, we get

$$(\hbar\Omega_\lambda-\hbar\omega)\check{B}_\lambda(\omega)$$
$$=\sum_{\mu,\nu}F_{\lambda,\mu,\nu}^*\int_{-\infty}^\infty\mathrm{d}\omega'\,(\hbar\omega_\nu-\hbar\omega')\check{b}_\nu(\omega')\check{b}_\mu(\omega-\omega'). \quad (20)$$

In principle, the biexciton RHPS process is described by the three equations of motion (9), (19), and (20), and commutation relations (10) and (12). However, in the actual calculation, we use the following approximation.

C. Approximation for RHPS process

We suppose that a coherent light beam resonantly excites biexcitons and their amplitude is large enough compared to the vacuum fluctuation. In this situation, if we do not consider the other higher processes, the biexciton operator in the nonlinear term of Eq. (19) can be replaced by its amplitude $\mathcal{B}_\lambda(\omega')=\langle\check{B}_\lambda(\omega')\rangle$. Further, we replace $\check{b}_\nu(\omega'-\omega)$ in the nonlinear term by $\check{b}_\nu^{(1)}(\omega'-\omega)$, which

satisfies the linear equation

$$[\hbar\omega_\mu - \hbar\omega - i\gamma_{ex}/2]\, \check{b}_\mu^{(1)}(\omega)$$

$$= \int d\boldsymbol{r}\, \boldsymbol{\mathcal{P}}_\mu^*(\boldsymbol{r}) \cdot \check{\boldsymbol{E}}^+(\boldsymbol{r},\omega) + \check{\mathcal{D}}_\mu(\omega). \qquad (21)$$

Simultaneously solving this equation and Eq. (9), $\check{b}_\mu^{(1)}(\omega)$ can be expressed by the fluctuation operators $\check{\boldsymbol{J}}_0(\boldsymbol{r},\omega)$

and $\check{\mathcal{D}}_\mu(\omega)$. Its calculation is straightforward by using the Green's function technique as will be shown in section II E. Under the above approximation, Eq. (19) is rewritten as

$$[\hbar\omega_\mu - \hbar\omega - i\gamma_{ex}/2]\, \check{b}_\mu(\omega) \simeq \int d\boldsymbol{r}\, \boldsymbol{\mathcal{P}}_\mu^*(\boldsymbol{r}) \cdot \check{\boldsymbol{E}}^+(\boldsymbol{r},\omega) + \check{\mathcal{D}}_\mu(\omega)$$

$$+ \sum_{\lambda,\nu} (\hbar\omega_\mu + \hbar\omega_\nu - \hbar\Omega_\lambda) F_{\lambda,\mu,\nu} \int_{-\infty}^\infty d\omega'\, \{\check{b}_\nu^{(1)}(\omega' - \omega)\}^\dagger \mathcal{B}_\lambda(\omega'). \qquad (22)$$

By solving this equation and Eq. (9), we can represent $\check{\boldsymbol{E}}^+(\boldsymbol{r},\omega)$ by the fluctuation operators $\check{\boldsymbol{J}}_0(\boldsymbol{r},\omega)$ and $\check{\mathcal{D}}_\mu(\omega)$. This calculation is also straightforward by using the Green's function.

For the calculation of $\mathcal{B}_\lambda(\omega)$, we suppose that the biexciton amplitude is not decreased by the scattering, because its contribution is small compared to the pumping light. Under this approximation, by phenomenologically introducing a damping constant γ_{bx}, the biexciton amplitude is obtained from Eq. (20) as

$$\mathcal{B}_\lambda(\omega) \simeq \frac{1}{\hbar\Omega_\lambda - \hbar\omega - i\gamma_{bx}/2} \sum_{\mu,\nu} F_{\lambda,\mu,\nu}^*$$

$$\times \int_{-\infty}^\infty d\omega'\, (\hbar\omega_\nu - \hbar\omega') \langle \check{b}_\nu^{(1)}(\omega') \rangle \langle \check{b}_\mu^{(1)}(\omega - \omega') \rangle, \quad (23)$$

where $\langle \check{b}_\nu^{(1)}(\omega') \rangle$ can be calculated from Eqs. (9) and (21) by considering an incident light beam as a homogeneous solution of Eq. (9). Under the weak bipolariton regime,[16] where the coupling between exciton-polariton and biexciton is small enough compared to their broadening, the approximated expression (23) of biexciton amplitude is sufficient for the discussion of RHPS process. While Savasta et al. considered the equation of motion of projection operators,[12,39] they also used a similar approximation for the treatment of biexcitons under the detailed verification of its validity.

D. Model of biexcitons

Although $F_{\lambda,\mu,\nu}$ and Ω_λ should be in principle determined from Eq. (17) for given nonlinear coefficient $V_{\mu,\nu;\mu',\nu'}$, we instead express $F_{\lambda,\mu,\nu}$ and Ω_λ by using experimental results. This treatment is useful because we already know many parameters of the lowest level of biexcitons in CuCl by the longstanding experimental and theoretical studies.[11]

It is well known that the lowest level of biexcitons in CuCl is singlet and has zero angular momentum, because of the exchange interactions between two electrons and between two holes.[11] Since we suppose the resonant two-photon excitation of the lowest level, we only consider the lowest relative motion of biexciton in our calculation. Further, according to the RHPS experiments in Ref. 54, the lowest biexciton state mainly consists of $1s$ excitons, and the contribution from the higher exciton states was estimated in the order of 10^{-4}. Therefore, we consider only $1s$ relative motion of excitons, which has a degree of freedom of polarization direction $\xi_\mu = \{x, y, z\}$. According to the exciton and biexciton states in bulk CuCl,[11] the lowest biexciton level $|J = 0, M = 0\rangle_{bx}$ with zero angular momentum is represented as

$$|J = 0, M = 0\rangle_{bx} = \frac{1}{2}\{|0,0;0,0\rangle_{2ex} + |1,1;1,-1\rangle_{2ex}$$
$$+ |1,-1;1,1\rangle_{2ex} - |1,0;1,0\rangle_{2ex}\}, \tag{24}$$

where $|j_1, m_1; j_2, m_2\rangle_{2ex}$ is the two-exciton state represented in terms of angular momenta (j_1, m_1) and (j_2, m_2) of two excitons. This expression surely reflects the polarization correlation of photon pairs observed in RHPS experiments[10,13] and also determines the phase between the two states

$$\Phi_+ = (|L, R\rangle + |R, L\rangle)/\sqrt{2} \tag{25a}$$

$$= (|H, H\rangle + |V, V\rangle)/\sqrt{2}. \tag{25b}$$

Here, $|L, R\rangle$ means that one photon is left- and the other is right-circularly polarized, and $|R, L\rangle$ is the opposite state. $|H, H\rangle$ and $|V, V\rangle$ respectively means that both photons are horizontally and vertically polarized. By rewriting each exciton state in terms of the polarization

direction as

$$|j, m\rangle = \begin{cases} |1, 1\rangle = -\left(|x\rangle + \mathrm{i}|y\rangle\right)/\sqrt{2}, \\ |1, 0\rangle = |z\rangle, \\ |1, -1\rangle = \left(|x\rangle - \mathrm{i}|y\rangle\right)/\sqrt{2}, \end{cases} \quad (26)$$

Eq. (24) is rewritten as

$$|J = 0, M = 0\rangle_{\mathrm{bx}}$$
$$= \frac{1}{2}\{|0, 0; 0, 0\rangle_{2\mathrm{ex}} - |x; x\rangle_{2\mathrm{ex}} - |y; y\rangle_{2\mathrm{ex}} - |z; z\rangle_{2\mathrm{ex}}\}, \quad (27)$$

which also reflects the polarization correlation (25b).

Considering the relative motion $\Psi(\boldsymbol{r})$ of two excitons in the lowest biexciton level, the coefficient is written as

$$F_{\lambda,\mu,\nu} = \delta_{\lambda,\mu,\nu} \int \mathrm{d}\boldsymbol{r} \int \mathrm{d}\boldsymbol{r}' \, \Psi(\boldsymbol{r}') g_\lambda^{\mathrm{bx}}(\boldsymbol{r}) g_\mu^{\mathrm{ex}*}(\boldsymbol{r}+\boldsymbol{r}') g_\nu^{\mathrm{ex}*}(\boldsymbol{r}), \quad (28)$$

where $g_m^{\mathrm{ex}}(\boldsymbol{r})$ and $g_l^{\mathrm{bx}}(\boldsymbol{r})$ are center-of-mass wavefunctions of excitons and biexcitons, respectively, and

$$\delta_{\lambda,\mu,\nu} = \delta_{\xi_\mu, \xi_\nu} \quad (29)$$

represents the polarization selection rule reflecting the lowest state of biexciton [Eq. (27)]. Here, we suppose that the Bohr radius of biexciton (1.5 nm in CuCl)[65] is much smaller than the crystal size, and the relative motion of biexcitons is not strongly modified from the bulk one. Namely, we approximate the above expression as

$$F_{\lambda,\mu,\nu} \simeq \delta_{\lambda,\mu,\nu} \Phi \int \mathrm{d}\boldsymbol{r} \, g_\lambda^{\mathrm{bx}}(\boldsymbol{r}) \, g_\mu^{\mathrm{ex}*}(\boldsymbol{r}) \, g_\nu^{\mathrm{ex}*}(\boldsymbol{r}), \quad (30)$$

where Φ is defined as

$$\Phi \equiv \int \mathrm{d}\boldsymbol{r} \, \Psi(\boldsymbol{r}). \quad (31)$$

$|\Phi|^2$ represents the effective volume of the lowest biexciton state. It was estimated by an experiment,[53] and was also used as a parameter in a theoretical work.[66]

E. Green's function technique

Here, we explain how we simultaneously solve the equation of motion of electric field [Eq. (9)] and that of excitons [Eq. (21) or Eq. (22)]. By using the dyadic Green's function satisfying

$$\boldsymbol{\nabla} \times \boldsymbol{\nabla} \times \overleftrightarrow{\mathbf{G}}(\boldsymbol{r}, \boldsymbol{r}', \omega) - \frac{\omega^2}{c^2}\varepsilon_{\mathrm{bg}}(\boldsymbol{r}, \omega)\overleftrightarrow{\mathbf{G}}(\boldsymbol{r}, \boldsymbol{r}', \omega) = \delta(\boldsymbol{r}-\boldsymbol{r}')\overleftrightarrow{\mathbf{1}}, \quad (32)$$

we can rewrite Eq. (9) as

$$\check{\boldsymbol{E}}^+(\boldsymbol{r}, \omega) = \check{\boldsymbol{E}}_0^+(\boldsymbol{r}, \omega) + \mu_0\omega^2 \int \mathrm{d}\boldsymbol{r}' \, \overleftrightarrow{\mathbf{G}}(\boldsymbol{r}, \boldsymbol{r}', \omega)\cdot\check{\boldsymbol{P}}_{\mathrm{ex}}^+(\boldsymbol{r}', \omega), \quad (33)$$

where $\check{\boldsymbol{E}}_0^+(\boldsymbol{r}, \omega)$ represents the electric field in the background ($\hat{H}_{\mathrm{em}}$) system, and it is defined as

$$\check{\boldsymbol{E}}_0^+(\boldsymbol{r}, \omega) \equiv \mathrm{i}\mu_0\omega \int \mathrm{d}\boldsymbol{r}' \, \overleftrightarrow{\mathbf{G}}(\boldsymbol{r}, \boldsymbol{r}', \omega) \cdot \check{\boldsymbol{J}}_0(\boldsymbol{r}', \omega). \quad (34)$$

From Eq. (10), $\check{\boldsymbol{E}}_0^+(\boldsymbol{r}, \omega)$ satisfies[44]

$$\left[\check{\boldsymbol{E}}_0^+(\boldsymbol{r}, \omega), \check{\boldsymbol{E}}_0^-(\boldsymbol{r}', \omega')\right] = \left[\check{\boldsymbol{E}}_0^+(\boldsymbol{r}, \omega), \check{\boldsymbol{E}}_0^+(\boldsymbol{r}', -\omega')\right]$$
$$= \delta(\omega - \omega')\frac{\mu_0\hbar\omega^2}{\mathrm{i}2\pi}[\overleftrightarrow{\mathbf{G}}(\boldsymbol{r}, \boldsymbol{r}', \omega) - \overleftrightarrow{\mathbf{G}}^*(\boldsymbol{r}, \boldsymbol{r}', \omega)]. \quad (35)$$

The expression of $\overleftrightarrow{\mathbf{G}}(\boldsymbol{r}, \boldsymbol{r}', \omega)$ in planar system (dielectric multilayer) is already known[67] and will be shown in Sec. III.

Substituting Eq. (33) into Eq. (22), we obtain the simultaneous equation set for exciton operators under the rotating-wave approximation (RWA) as

$$\sum_{\mu'} S_{\mu,\mu'}(\omega)\check{b}_{\mu'}(\omega) = \int \mathrm{d}\boldsymbol{r} \, \boldsymbol{\mathcal{P}}_\mu^*(\boldsymbol{r}) \cdot \check{\boldsymbol{E}}_0^+(\boldsymbol{r}, \omega) + \check{\mathcal{D}}_\mu(\omega)$$
$$+ \sum_{\lambda,\nu}(\hbar\omega_\mu + \hbar\omega_\nu - \hbar\Omega_\lambda)F_{\lambda,\mu,\nu}\int_{-\infty}^{\infty}\mathrm{d}\omega' \, \{\check{b}_\nu^{(1)}(\omega' - \omega)\}^\dagger \mathcal{B}_\lambda(\omega'), \quad (36)$$

where the coefficient on the left-hand side is defined as

$$S_{\mu,\mu'}(\omega) \equiv [\hbar\omega_\mu - \hbar\omega - \mathrm{i}\gamma_{\mathrm{ex}}/2]\,\delta_{\mu,\mu'} - \mu_0\omega^2 \int \mathrm{d}\boldsymbol{r} \int \mathrm{d}\boldsymbol{r}' \, \boldsymbol{\mathcal{P}}_\mu^*(\boldsymbol{r}) \cdot \overleftrightarrow{\mathbf{G}}(\boldsymbol{r}, \boldsymbol{r}', \omega) \cdot \boldsymbol{\mathcal{P}}_{\mu'}(\boldsymbol{r}'). \quad (37)$$

The last term of Eq. (37) represents the self energy due to the retarded interaction through the electromagnetic

fields and the longitudinal Coulomb interaction. Further, Eq. (21) for $\check{b}_\mu^{(1)}(\omega)$ in the linear regime is also rewritten as

$$\sum_{\mu'} S_{\mu,\mu'}(\omega)\check{b}_{\mu'}^{(1)}(\omega) = \int \mathrm{d}\boldsymbol{r} \; \boldsymbol{\mathcal{P}}_\mu^*(\boldsymbol{r}) \cdot \check{\boldsymbol{E}}_0^+(\boldsymbol{r},\omega) + \check{\mathcal{D}}_\mu(\omega).$$
(38)

This simultaneous linear equation set is solved by calculating the inverse matrix $\overleftrightarrow{\boldsymbol{W}}(\omega) = [\overleftrightarrow{\boldsymbol{S}}(\omega)]^{-1}$, and the commutation relation of $\check{b}_\mu^{(1)}(\omega)$ is derived in Ref. 44 as

$$\left[\check{b}_\mu^{(1)}(\omega), \{\check{b}_{\mu'}^{(1)}(\omega'^*)\}^\dagger \right]$$

$$= \delta(\omega - \omega')\frac{\hbar}{\mathrm{i}2\pi} \left[W_{\mu,\mu'}(\omega) - W_{\mu',\mu}^*(\omega) \right],$$ (39a)

$$\left[\check{b}_\mu^{(1)}(\omega), \check{b}_{\mu'}^{(1)}(-\omega') \right] = 0.$$ (39b)

Further, Eq. (36) is rewritten as

$$\check{b}_\mu(\omega) \simeq \check{b}_\mu^{(1)}(\omega) + \sum_{\mu',\lambda,\nu} W_{\mu,\mu'}(\omega)(\hbar\omega_{\mu'} + \hbar\omega_\nu - \hbar\Omega_\lambda)$$

$$\times F_{\lambda,\mu',\nu} \int_{-\infty}^\infty \mathrm{d}\omega' \; \{\check{b}_\nu^{(1)}(\omega' - \omega)\}^\dagger \mathcal{B}_\lambda(\omega'),$$ (40)

and, by substituting this into Eq. (33), the electric field involved with RHPS is expressed under the RWA and the approximations discussed in Sec. II C as

$$\check{\boldsymbol{E}}^+(\boldsymbol{r},\omega) \simeq \check{\boldsymbol{E}}_0^+(\boldsymbol{r},\omega) + \sum_\mu \boldsymbol{\mathcal{E}}_\mu(\boldsymbol{r},\omega)\check{b}_\mu^{(1)}(\omega) + \check{\boldsymbol{E}}_{\mathrm{NL}}(\boldsymbol{r},\omega),$$
(41)

where

$$\boldsymbol{\mathcal{E}}_\mu(\boldsymbol{r},\omega) \equiv \mu_0\omega^2 \int \mathrm{d}\boldsymbol{r}' \; \overleftrightarrow{\boldsymbol{G}}(\boldsymbol{r},\boldsymbol{r}',\omega) \cdot \boldsymbol{\mathcal{P}}_\mu(\boldsymbol{r}'),$$ (42)

$$\check{\boldsymbol{E}}_{\mathrm{NL}}^+(\boldsymbol{r},\omega) = \sum_{\mu,\mu',\lambda,\nu} \boldsymbol{\mathcal{E}}_\mu(\boldsymbol{r},\omega)W_{\mu,\mu'}(\omega)(\hbar\omega_{\mu'} + \hbar\omega_\nu - \hbar\Omega_\lambda)$$

$$\times F_{\lambda,\mu',\nu} \int_{-\infty}^\infty \mathrm{d}\omega' \; \{\check{b}_\nu^{(1)}(\omega' - \omega)\}^\dagger \mathcal{B}_\lambda(\omega').$$
(43)

F. Input and output fields

Here, we must pay attention to the electric field $\check{\boldsymbol{E}}_0^+(\boldsymbol{r},\omega)$ in the background system, which represents not only the field from matter to an observing point $\boldsymbol{r}$ but also the field from $\boldsymbol{r}$ to the matter. This means that the latter contribution must be removed from Eq. (41) to calculate observables, while the other terms involving $\check{b}_\mu^{(1)}(\omega)$ and $\check{\boldsymbol{E}}_{\mathrm{NL}}(\boldsymbol{r},\omega)$ represents the components emitted from the matter. While such a calculation has been usually treated by the input-output relations,[41,59–63] we use the following treatment based on the dyadic Green's function $\overleftrightarrow{\boldsymbol{G}}(\boldsymbol{r},\boldsymbol{r}',\omega)$ for $\check{\boldsymbol{E}}_0^+(\boldsymbol{r},\omega)$.

We separate $\check{\boldsymbol{E}}_0^+(\boldsymbol{r},\omega)$ into an input field $\check{\boldsymbol{E}}_{0,\mathrm{IN}}^+(\boldsymbol{r},\omega)$ from $\boldsymbol{r}$ to the matter and an output field $\check{\boldsymbol{E}}_{0,\mathrm{OUT}}^+(\boldsymbol{r},\omega)$ from the matter to $\boldsymbol{r}$ as

$$\check{\boldsymbol{E}}_0^+(\boldsymbol{r},\omega) = \check{\boldsymbol{E}}_{0,\mathrm{IN}}^+(\boldsymbol{r},\omega) + \check{\boldsymbol{E}}_{0,\mathrm{OUT}}^+(\boldsymbol{r},\omega).$$ (44)

By considering the causality, the output field at time t should have a correlation only with fields at $t' < t$, and the commutation relation should be written as

$$\left[\check{\boldsymbol{E}}_{0,\mathrm{OUT}}^+(\boldsymbol{r},\omega), \check{\boldsymbol{E}}_0^-(\boldsymbol{r}',\omega') \right]$$

$$= \frac{1}{(2\pi)^2} \int_{-\infty}^\infty \mathrm{d}t' \int_{t'}^\infty \mathrm{d}t \; \mathrm{e}^{\mathrm{i}\omega t - \mathrm{i}\omega' t'} \left[\hat{\boldsymbol{E}}_0(\boldsymbol{r},t), \hat{\boldsymbol{E}}_0(\boldsymbol{r}',t') \right]$$

$$= \delta(\omega - \omega')\frac{\mu_0\hbar\omega^2}{\mathrm{i}2\pi}\overleftrightarrow{\boldsymbol{G}}(\boldsymbol{r},\boldsymbol{r}',\omega),$$ (45)

where we use the fact that the dyadic Green's function $\overleftrightarrow{\boldsymbol{G}}(\boldsymbol{r},\boldsymbol{r}',\omega)$ satisfying Eq. (32) is the retarded correlation function of the electric field:[44,68]

$$- \mu_0\omega^2\overleftrightarrow{\boldsymbol{G}}(\boldsymbol{r},\boldsymbol{r}',\omega)$$

$$= \frac{1}{\mathrm{i}\hbar} \int_{t'}^\infty \mathrm{d}t \; \mathrm{e}^{\mathrm{i}\omega(t-t')} \left\langle \left[\hat{\boldsymbol{E}}_0(\boldsymbol{r},t), \hat{\boldsymbol{E}}_0(\boldsymbol{r}',t') \right] \right\rangle.$$ (46)

In the same manner, the input field at t should have a correlation only with fields at $t' > t$, and the commutation relation is derived as

$$\left[\check{\boldsymbol{E}}_{0,\mathrm{IN}}^+(\boldsymbol{r},\omega), \check{\boldsymbol{E}}_0^-(\boldsymbol{r}',\omega') \right]$$

$$= \frac{1}{(2\pi)^2} \int_{-\infty}^\infty \mathrm{d}t' \int_{-\infty}^{t'} \mathrm{d}t \; \mathrm{e}^{\mathrm{i}\omega t - \mathrm{i}\omega' t'} \left[\hat{\boldsymbol{E}}_0(\boldsymbol{r},t), \hat{\boldsymbol{E}}_0(\boldsymbol{r}',t') \right]$$

$$= -\delta(\omega - \omega')\frac{\mu_0\hbar\omega^2}{\mathrm{i}2\pi}\overleftrightarrow{\boldsymbol{G}}^*(\boldsymbol{r},\boldsymbol{r}',\omega).$$ (47)

Actually, Eqs. (45) and (47) reproduces Eq. (35). By using the output field $\check{\boldsymbol{E}}_{0,\mathrm{OUT}}^+(\boldsymbol{r},\omega)$ in the background system, we define the scattering field excluding the input one as

$$\check{\boldsymbol{E}}_{\mathrm{RHPS}}^+(\boldsymbol{r},\omega) \equiv \check{\boldsymbol{E}}^+(\boldsymbol{r},\omega) - \check{\boldsymbol{E}}_{0,\mathrm{IN}}^+(\boldsymbol{r},\omega)$$

$$= \check{\boldsymbol{E}}_{\mathrm{LIN}}^+(\boldsymbol{r},\omega) + \check{\boldsymbol{E}}_{\mathrm{NL}}^+(\boldsymbol{r},\omega),$$ (48)

where $\check{\boldsymbol{E}}_{\mathrm{LIN}}^+(\boldsymbol{r},\omega)$ is the linear component of the electric field excluding the input field as

$$\check{\boldsymbol{E}}_{\mathrm{LIN}}^+(\boldsymbol{r},\omega) = \check{\boldsymbol{E}}_{0,\mathrm{OUT}}^+(\boldsymbol{r},\omega) + \sum_\mu \boldsymbol{\mathcal{E}}_\mu(\boldsymbol{r},\omega)\check{b}_\mu^{(1)}(\omega).$$ (49)

By deriving commutation relations of $\check{\boldsymbol{E}}_{\mathrm{LIN}}(\boldsymbol{r},\omega)$ and $\check{\boldsymbol{E}}_{\mathrm{NL}}(\boldsymbol{r},\omega)$ from Eqs. (35), (39), and (45), we can evaluate the observables of RHPS.

III. PRACTICAL CALCULATION

Next, we apply the theoretical framework discussed in the previous section into multilayer systems embedding
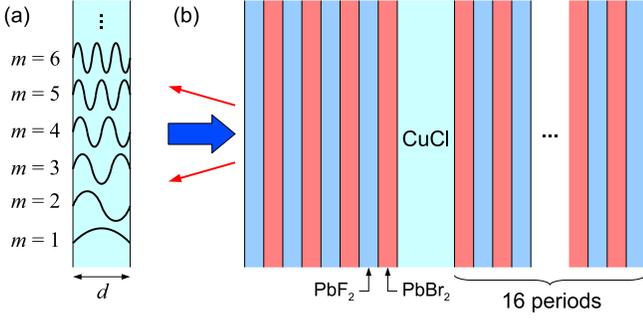
FIG. 2: (a) Center-of-mass wavefunctions of excitons and biexcitons in a CuCl film. Simple sinusoidal functions vanishing at surfaces are supposed. (b) Cavity structure considered in Figs. 9 and 10. The Bragg mirrors consist of PbBr$_2$ and PbF$_2$. On the transmission side, a high reflectance is achieved by a mirror with 16 periods to suppress the leakage of photons in this direction. On the incident side, only 4 periods are supposed to guarantee rapid radiative decay of entangled photons.

a CuCl layer, and derive expressions of one-photon scattering intensity and two-photon coincidence intensity by RHPS. An incident light beam propagates along z axis (perpendicular to the surface), and photon pairs emitted into $x - z$ plane are considered (in-plane vector is in x direction). We suppose that center-of-mass motions of excitons and biexcitons are confined in the CuCl layer with thickness d existing at $0 < z < d$. Since we consider a large enough thickness d compared to the Bohr radii of exciton (0.7 nm) and biexciton (1.5 nm),[65] the relative motions of excitons and biexcitons are not strongly modified from the ones in bulk crystals, and all the information of the relative motions are described by factors M and Φ in Eqs. (8) and (30). As seen in Fig. 2(a), the center-of-mass wavefunctions of excitons and biexcitons are expanded by a series of sinusoidal functions as

$$g_{\bar{k},m}^{\mathrm{bx}}(\boldsymbol{r}) = g_{\bar{k},m}^{\mathrm{ex}}(\boldsymbol{r}) = \theta(z)\frac{\mathrm{e}^{\mathrm{i}\bar{k}x}}{\sqrt{S}}\sqrt{\frac{2}{d}}\sin(q_m z), \quad (50)$$

where $\theta(z)$ is unity for $0 < z < d$ and zero otherwise, $\bar{k}$ is the in-plane wavenumber, S is the normalization area in $x - y$ plane, and $q_m = m\pi/d$ is the confinement wavenumber in z direction for $m = 1$, 2, ... We consider $\varepsilon_{\mathrm{bg}}(\boldsymbol{r},\omega)$ as a discontinuous step-like function in z direction representing the background dielectric constant in each layer, and it does not depend on ω nor $\boldsymbol{r}_\parallel$. In the case of multilayer structure in Fig. 2(b), $\varepsilon_{\mathrm{bg}}(\boldsymbol{r},\omega)$ gives the background dielectric constant $\varepsilon_{\mathrm{bg}}^{\mathrm{ex}}$ for excitons at CuCl layer, otherwise it gives the dielectric constant of each layer. According to Ref. 67, if z' is in the CuCl layer, the dyadic Green's function satisfying Eq. (32) is

expressed as

$$\overleftrightarrow{\mathbf{G}}_{\bar{k}}(z,z',\omega) \equiv \int \mathrm{d}\boldsymbol{r}_\parallel \int \mathrm{d}\boldsymbol{r}_\parallel' \frac{\mathrm{e}^{-\mathrm{i}\bar{k}(x-x')}}{S}\overleftrightarrow{\mathbf{G}}(\boldsymbol{r},\boldsymbol{r}',\omega)$$
$$= -\frac{1}{\mathrm{i}2k_{\mathrm{bg}}^{\mathrm{ex}}}\left[\overleftrightarrow{\boldsymbol{\mathcal{G}}}_{\bar{k}}^V(z,z',\omega) + \overleftrightarrow{\boldsymbol{\mathcal{G}}}_{\bar{k}}^H(z,z',\omega)\right]$$
$$- \frac{\boldsymbol{e}_z\boldsymbol{e}_z}{\varepsilon_{\mathrm{bg}}^{\mathrm{ex}}\omega^2/c^2}\delta(z-z'), \quad (51)$$

where $k_{\mathrm{bg}}^{\mathrm{ex}\,2} = \varepsilon_{\mathrm{bg}}^{\mathrm{ex}}\omega^2/c^2 - \bar{k}^2$ and $\boldsymbol{e}_\xi$ is the unit vector in ξ direction. When z is in layer j with dielectric constant ε_i, the tensors in Eq. (51) are written as

$$\overleftrightarrow{\boldsymbol{\mathcal{G}}}_{\bar{k}}^V(z,z',\omega) = \boldsymbol{e}_y\boldsymbol{e}_y\mathcal{G}_{\bar{k}}^V(z,z',\omega), \quad (52)$$

$$\overleftrightarrow{\boldsymbol{\mathcal{G}}}_{\bar{k}}^H(z,z',\omega) = \begin{pmatrix} \mathrm{D}_z\mathrm{D}_z' & 0 & \mathrm{i}\mathrm{D}_z\bar{k} \\ 0 & 0 & 0 \\ -\mathrm{i}\bar{k}\mathrm{D}_z' & 0 & \bar{k}^2 \end{pmatrix}\frac{\mathcal{G}_{\bar{k}}^H(z,z',\omega)}{\sqrt{\varepsilon_{\mathrm{bg}}^{\mathrm{ex}}\varepsilon_j}\omega^2/c^2}, \quad (53)$$

where $\mathrm{D}_z \equiv \partial/\partial z$ and $\mathrm{D}_z' \equiv \partial/\partial z'$. Eqs. (52) and (53) respectively describe the propagation of V- and H-polarized fields, and, according to Ref. 67, $\mathcal{G}_{\bar{k}}^{V/H}(z,z')$ is expressed as follows. When $0 < z < d$ is in the CuCl layer,

$$\mathcal{G}_{\bar{k}}^{V/H}(z,z')$$
$$= \mathrm{e}^{\mathrm{i}k_{\mathrm{bg}}^{\mathrm{ex}}|z-z'|} + \mathrm{e}^{\mathrm{i}k_{\mathrm{bg}}^{\mathrm{ex}}z}\tilde{R}_L^{V/H}\left[\mathrm{e}^{\mathrm{i}k_{\mathrm{bg}}^{\mathrm{ex}}z'} + \tilde{R}_R^{V/H}\mathrm{e}^{\mathrm{i}k_{\mathrm{bg}}^{\mathrm{ex}}(2d-z')}\right]\tilde{M}^{V/H}$$
$$+ \mathrm{e}^{-\mathrm{i}k_{\mathrm{bg}}^{\mathrm{ex}}(z-d)}\tilde{R}_R^{V/H}\left[\mathrm{e}^{\mathrm{i}k_{\mathrm{bg}}^{\mathrm{ex}}(d-z')} + \tilde{R}_L^{V/H}\mathrm{e}^{\mathrm{i}k_{\mathrm{bg}}^{\mathrm{ex}}(d+z')}\right]\tilde{M}^{V/H}. \quad (54a)$$

When z is in the leftmost semi-infinite region,

$$\mathcal{G}_{\bar{k}}^{V/H}(z,z') = \mathrm{e}^{-\mathrm{i}k_L z}\tilde{T}_L^{V/H}\left[\mathrm{e}^{\mathrm{i}k_{\mathrm{bg}}^{\mathrm{ex}}z'} + \tilde{R}_R^{V/H}\mathrm{e}^{\mathrm{i}k_{\mathrm{bg}}^{\mathrm{ex}}(2d-z')}\right]\tilde{M}^{V/H}. \quad (54b)$$

When z is in the rightmost semi-infinite region,

$$\mathcal{G}_{\bar{k}}^{V/H}(z,z') = \mathrm{e}^{\mathrm{i}k_R z}\tilde{T}_R^{V/H}\left[\mathrm{e}^{\mathrm{i}k_{\mathrm{bg}}^{\mathrm{ex}}(d-z')} + \tilde{R}_L^{V/H}\mathrm{e}^{\mathrm{i}k_{\mathrm{bg}}^{\mathrm{ex}}(d+z')}\right]\tilde{M}^{V/H}. \quad (54c)$$

Here, $\tilde{R}_{L(R)}^{V/H}$ represents the generalized reflection coefficient for V/H-polarized field from the CuCl layer against the left(right)-hand neighboring, and $\tilde{T}_{L(R)}^{V/H}$ is the generalized transmission coefficient from the CuCl layer to the left(right)most region. The derivation of these coefficients is shown in Ref. 67. Further, $k_{L(R)}^2 = \varepsilon_{L(R)}\omega^2/c^2 - \bar{k}^2$ is the wavenumber in the left(right)most region with dielectric constant $\varepsilon_{L(R)}$, and the factor is defined as $\tilde{M}^{V/H} = [1 - \tilde{R}_L^{V/H}\tilde{R}_R^{V/H}\mathrm{e}^{\mathrm{i}2k_{\mathrm{bg}}^{\mathrm{ex}}d}]^{-1}$.

From Eqs. (50) and (51), we can evaluate the coefficient matrix $\overleftrightarrow{\mathbf{S}}(\omega)$ [Eq. (37)] and numerically calculate the inverse matrix $\overleftrightarrow{\mathbf{W}}(\omega) = [\overleftrightarrow{\mathbf{S}}(\omega)]^{-1}$. From Eq. (38), the amplitude of excitons is obtained in linear regime by

$$\langle \check{b}_\mu^{(1)}(\omega)\rangle = \sum_{\mu'} W_{\mu,\mu'}(\omega)\int \mathrm{d}\boldsymbol{r}\,\boldsymbol{\mathcal{P}}_{\mu'}^*(\boldsymbol{r})\cdot\langle \check{\boldsymbol{E}}_0^+(\boldsymbol{r},\omega)\rangle. \quad (55)$$

Here, $\langle \check{\boldsymbol{E}}_0^+(\boldsymbol{r},\omega)\rangle$ represents the amplitude of electric field in the background dielectric system $\hat{H}_{\mathrm{em}}$, and can be derived by the standard transfer matrix method[67] in the case of dielectric multilayers. For simplicity, we consider a monochromatic laser light with frequency ω_{in} with in-plane wavenumber $\bar{k}_{\mathrm{in}}$. Concerning the pump power I_{in} ($\langle \check{\boldsymbol{E}}_0^+\rangle \propto \sqrt{I_{\mathrm{in}}}$), there is a scaling law for the intensity of entangled photons as explained below. In the present paper, since we only consider the $1s$ exciton and the lowest biexciton level, the exciton states are labeled by polarization direction $\xi = \{x,y,z\}$, in-plane wavenumber $\bar{k}$, and index of center-of-mass motion m as $\mu = \{\xi,\bar{k},m\}$, and the biexciton states are labeled by $\lambda = \{\bar{k},m\}$. Considering the conservation of energy and in-plane wavevector, the amplitude of biexcitons is evaluated by Eq. (23) and we write it as

$$\mathcal{B}_{\bar{k},m}(\omega) = \delta_{\bar{k},2\bar{k}_{\mathrm{in}}}\delta(\omega - 2\omega_{\mathrm{in}})\tilde{\mathcal{B}}_{2\bar{k}_{\mathrm{in}},m}(2\omega_{\mathrm{in}}). \qquad (56)$$

Further, the linear and nonlinear components of the scattering field [Eqs. (49) and (43)] are simply rewritten as

$$\check{\boldsymbol{E}}_{\mathrm{LIN},\bar{k}}^+(z,\omega) = \frac{1}{\sqrt{S}}\int d\boldsymbol{r}_{\parallel}\ e^{-i\bar{k}x}\check{\boldsymbol{E}}_{\mathrm{LIN}}^+(\boldsymbol{r},\omega) = \check{\boldsymbol{E}}_{0,\mathrm{OUT},\bar{k}}^+(z,\omega) + \sum_{\xi,m}\boldsymbol{\mathcal{E}}_{\xi,\bar{k},m}(z,\omega)\check{b}_{\xi,\bar{k},m}^{(1)}(\omega), \qquad (57)$$

$$\check{\boldsymbol{E}}_{\mathrm{NL},\bar{k}}^+(z,\omega) = \frac{1}{\sqrt{S}}\int d\boldsymbol{r}_{\parallel}\ e^{-i\bar{k}x}\check{\boldsymbol{E}}_{\mathrm{NL}}^+(\boldsymbol{r},\omega) = \sum_{\xi,m}\boldsymbol{\mathcal{E}}_{\xi,\bar{k}_{\mathrm{in}},\bar{k},m}^{\mathrm{NL}}(z,\omega_{\mathrm{in}},\omega)\{\check{b}_{\xi,2\bar{k}_{\mathrm{in}}-k,m}^{(1)}(2\omega_{\mathrm{in}}-\omega)\}^{\dagger}, \qquad (58)$$

where the coefficients are evaluated by the following quantities and functions

$$\boldsymbol{\mathcal{E}}_{\xi,\bar{k},m}(z,\omega) \equiv \mu_0\omega^2 M\sqrt{\frac{1}{d}}\int dz'\ \overleftrightarrow{\mathbf{G}}_{\bar{k}}(z,z',\omega)\cdot \boldsymbol{e}_{\xi}\sin(q_m z')\theta(z'), \qquad (59)$$

$$\boldsymbol{\mathcal{E}}_{\xi,\bar{k}_{\mathrm{in}},\bar{k},m}^{\mathrm{NL}}(z,\omega_{\mathrm{in}},\omega) = \sum_{\xi',\xi'',m',m'',n}\boldsymbol{\mathcal{E}}_{\xi'',\bar{k},m''}(z,\omega)W_{\{\xi'',\bar{k},m''\},\{\xi',\bar{k},m'\}}(\omega)$$
$$\times (\hbar\omega_{\xi',\bar{k},m'} + \hbar\omega_{\xi,2\bar{k}_{\mathrm{in}}-\bar{k},m} - \hbar\Omega_{2\bar{k}_{\mathrm{in}},n})F_{\{2\bar{k}_{\mathrm{in}},n\},\{\xi',\bar{k},m'\},\{\xi,2\bar{k}_{\mathrm{in}}-\bar{k},m\}}\tilde{\mathcal{B}}_{2\bar{k}_{\mathrm{in}},n}(2\omega_{\mathrm{in}}), \qquad (60)$$

$$F_{\{2\bar{k}_{\mathrm{in}},n\},\{\xi',\bar{k},m'\},\{\xi,\bar{k}',m\}} = \delta_{\xi,\xi'}\delta_{\bar{k}',2\bar{k}_{\mathrm{in}}-\bar{k}}\Phi\left(\frac{2}{d}\right)^{3/2}\int dz\ \theta(z)\sin(q_n z)\sin(q_m z)\sin(q_{m'} z), \qquad (61)$$

$$S_{\{\xi,\bar{k},m\},\{\xi',\bar{k}',m'\}}(\omega) = \left[\hbar\omega_{\xi,\bar{k},m} - \hbar\omega - i\gamma_{\mathrm{ex}}/2\right]\delta_{\xi,\xi'}\delta_{\bar{k},\bar{k}'}\delta_{m,m'}$$
$$- \delta_{\bar{k},\bar{k}'}\mu_0\omega^2|M|^2\int dz\int dz'\ \theta(z)\theta(z')\boldsymbol{e}_{\xi}\cdot\overleftrightarrow{\mathbf{G}}_{\bar{k}}(z,z',\omega)\cdot\boldsymbol{e}_{\xi'}\sin(q_m z)\sin(q_{m'} z'). \qquad (62)$$

Further, from the commutation relations (39) and (45), the following relations are derived for $\omega > 0$ and $\omega' > 0$ as

$$\left[\check{\boldsymbol{E}}_{\mathrm{LIN},\bar{k}}^+(\boldsymbol{r},\omega),\check{\boldsymbol{E}}_{\mathrm{NL},\bar{k}'}^+(\boldsymbol{r}',\omega')\right] = \delta_{\bar{k}',2\bar{k}_{\mathrm{in}}-\bar{k}}\delta(\omega+\omega'-2\omega_{\mathrm{in}})\overleftrightarrow{\mathbf{H}}_{\bar{k}_{\mathrm{in}},\bar{k}}^{\mathrm{LN}}(z,z',\omega_{\mathrm{in}},\omega), \qquad (63a)$$

$$\left[\check{\boldsymbol{E}}_{\mathrm{LIN},\bar{k}}^+(\boldsymbol{r},\omega),\check{\boldsymbol{E}}_{\mathrm{NL},\bar{k}'}^-(\boldsymbol{r}',\omega')\right] = \overleftrightarrow{\mathbf{0}}, \qquad (63b)$$

$$\left[\check{\boldsymbol{E}}_{\mathrm{NL},\bar{k}}^-(\boldsymbol{r},\omega),\check{\boldsymbol{E}}_{\mathrm{NL},\bar{k}'}^+(\boldsymbol{r}',\omega')\right] = \delta_{\bar{k},\bar{k}'}\delta(\omega-\omega')\overleftrightarrow{\mathbf{H}}_{\bar{k}_{\mathrm{in}},\bar{k}}^{\mathrm{NN}}(z,z',\omega_{\mathrm{in}},\omega), \qquad (64a)$$

$$\left[\check{\boldsymbol{E}}_{\mathrm{NL},\bar{k}}^+(\boldsymbol{r},\omega),\check{\boldsymbol{E}}_{\mathrm{NL},\bar{k}'}^+(\boldsymbol{r}',\omega')\right] = \overleftrightarrow{\mathbf{0}}, \qquad (64b)$$

where the tensors are defined as

$$\overleftrightarrow{\mathbf{H}}_{\bar{k}_{\mathrm{in}},\bar{k}}^{\mathrm{LN}}(z,z',\omega_{\mathrm{in}},\omega) \equiv \frac{\hbar}{i2\pi}\sum_{\xi,\xi',m,m'}\boldsymbol{\mathcal{E}}_{\xi,\bar{k},m}(z,\omega)W_{\{\xi,\bar{k},m\},\{\xi',\bar{k},m'\}}(\omega)\boldsymbol{\mathcal{E}}_{\xi',\bar{k}_{\mathrm{in}},2\bar{k}_{\mathrm{in}}-\bar{k},m'}^{\mathrm{NL}}(z',\omega_{\mathrm{in}},2\omega_{\mathrm{in}}-\omega), \qquad (65)$$

$$\overleftrightarrow{\mathbf{H}}^{\mathrm{NN}}_{\bar{k}_{\mathrm{in}},\bar{k}}(z,z',\omega_{\mathrm{in}},\omega) \equiv \frac{\hbar}{\mathrm{i}2\pi} \sum_{\xi,\xi',m,m'} \boldsymbol{\mathcal{E}}^{\mathrm{NL}*}_{\xi,\bar{k}_{\mathrm{in}},\bar{k},m}(z,\omega) \left[W_{\{\xi,2\bar{k}_{\mathrm{in}}-\bar{k},m\},\{\xi',2\bar{k}_{\mathrm{in}}-\bar{k},m'\}}(2\omega_{\mathrm{in}}-\omega) \right.$$

$$\left. - W^{*}_{\{\xi',2\bar{k}_{\mathrm{in}}-\bar{k},m'\},\{\xi,2\bar{k}_{\mathrm{in}}-\bar{k},m\}}(2\omega_{\mathrm{in}}-\omega) \right] \boldsymbol{\mathcal{E}}^{\mathrm{NL}}_{\xi',\bar{k}_{\mathrm{in}},\bar{k},m'}(z',\omega_{\mathrm{in}},\omega). \tag{66}$$

From these commutation relations, we calculate the one-photon scattering intensity and the two-photon coincidence intensity. When the background field $\check{\boldsymbol{E}}_{0,\bar{k}}(z)$ is in vacuum state in the scattering direction determined by $\bar{k}$ and only has the quantum fluctuation, we obtain the following relations for the initial condition $|0\rangle$ without considering the perturbation by the exciton-exciton scattering:

$$\check{\boldsymbol{E}}^{+}_{0,\bar{k}}(z,\omega)|0\rangle = \check{\boldsymbol{E}}^{+}_{0,\mathrm{OUT},\bar{k}}(z,\omega)|0\rangle = \check{\boldsymbol{E}}^{+}_{\mathrm{LIN},\bar{k}}(z,\omega)|0\rangle = \check{\boldsymbol{E}}^{-}_{\mathrm{NL},\bar{k}}(z,\omega)|0\rangle = \boldsymbol{0}. \tag{67}$$

When we measure the one-photon scattering intensity in the direction $\bar{k}$ at position z with polarization direction ξ and frequency ω by resolution $\Delta\omega$, the intensity is written as

$$C^{(1)}_{\xi,\bar{k}_{\mathrm{in}},\bar{k}}(z,\omega_{\mathrm{in}},\omega) = \int_{\omega-\Delta\omega/2}^{\omega+\Delta\omega/2} \mathrm{d}\omega'\mathrm{d}\omega'' \, \langle \check{E}^{-}_{\mathrm{RHPS},\bar{k},\xi}(z,\omega')\check{E}^{+}_{\mathrm{RHPS},\bar{k},\xi}(z,\omega'') \rangle$$

$$= \Delta\omega \left[\overleftrightarrow{\mathbf{H}}^{\mathrm{NN}}_{\bar{k}_{\mathrm{in}},\bar{k}}(z,z,\omega_{\mathrm{in}},\omega) \right]_{\xi,\xi}, \tag{68}$$

where $\check{E}^{\pm}_{\mathrm{RHPS},\bar{k},\xi}$ is the ξ component of $\check{\boldsymbol{E}}^{\pm}_{\mathrm{RHPS},\bar{k}}$ and $[\cdots]_{\xi,\xi'}$ extracts (ξ,ξ') component of the tensor. Here, it is worth noting that this one-photon scattering intensity is proportional to $I_{\mathrm{in}}{}^{2}$, the square of the pump power, reflecting the power dependence of the biexciton creation. Further, the z dependence of this function only represents the scattering direction to left or right hand side, if the leftmost and rightmost regions are non-absorptive. When we measure the two-photon coincidence between the scattering fields of $(\xi_1,\bar{k}_1,z_1,\omega_1)$ and $(\xi_2,\bar{k}_2,z_2,\omega_2)$, the intensity is calculated by

$$C^{(2)}_{\xi_1,\xi_2,\bar{k}_{\mathrm{in}},\bar{k}_1,\bar{k}_2}(z_1,z_2,\omega_{\mathrm{in}},\omega_1,\omega_2) = \int_{\omega_1-\Delta\omega/2}^{\omega_1+\Delta\omega/2} \mathrm{d}\omega_1'\mathrm{d}\omega_1'' \int_{\omega_2-\Delta\omega/2}^{\omega_2+\Delta\omega/2} \mathrm{d}\omega_2'\mathrm{d}\omega_2''$$

$$\times \langle \check{E}^{-}_{\mathrm{RHPS},\bar{k}_1,\xi_1}(z_1,\omega_1')\check{E}^{-}_{\mathrm{RHPS},\bar{k}_2,\xi_2}(z_2,\omega_2')\check{E}^{+}_{\mathrm{RHPS},\bar{k}_2,\xi_2}(z_2,\omega_2'')\check{E}^{+}_{\mathrm{RHPS},\bar{k}_1,\xi_1}(z_1,\omega_1'') \rangle. \tag{69}$$

By using the above commutation relations, we finally get

$$C^{(2)}_{\xi_1,\xi_2,\bar{k}_{\mathrm{in}},\bar{k}_1,\bar{k}_2}(z_1,z_2,\omega_{\mathrm{in}},\omega_1,\omega_2)$$

$$= \delta_{\bar{k}_2,2\bar{k}_{\mathrm{in}}-\bar{k}_1}\tilde{\delta}(\omega_1+\omega_2,2\omega_{\mathrm{in}})C^{(2)\mathrm{S}}_{\xi_1,\xi_2,\bar{k}_{\mathrm{in}},\bar{k}_1}(z_1,z_2,\omega_{\mathrm{in}},\omega_1) + C^{(2)\mathrm{N}}_{\xi_1,\xi_2,\bar{k}_{\mathrm{in}},\bar{k}_1,\bar{k}_2}(z_1,z_2,\omega_{\mathrm{in}},\omega_1,\omega_2)$$

$$+ (\Delta\omega)^2\delta_{\bar{k}_1,\bar{k}_2}\tilde{\delta}(\omega_1,\omega_2) \left[\overleftrightarrow{\mathbf{H}}^{\mathrm{NN}}_{\bar{k}_{\mathrm{in}},\bar{k}_1}(z_1,z_2,\omega_1) \right]_{\xi_1,\xi_2} \left[\overleftrightarrow{\mathbf{H}}^{\mathrm{NN}}_{\bar{k}_{\mathrm{in}},\bar{k}_2}(z_2,z_1,\omega_2) \right]_{\xi_2,\xi_1}. \tag{70}$$

Here, the function $\tilde{\delta}(\omega,\omega')$ gives unity for $\omega \simeq \omega'$ and zero otherwise. The first term represents the signal intensity, i.e., the number of correlated photon pairs, which satisfies the energy conservation $\omega_1+\omega_2 \simeq 2\omega_{\mathrm{in}}$ by resolution $\Delta\omega$, and the intensity is calculated as

$$C^{(2)\mathrm{S}}_{\xi_1,\xi_2,\bar{k}_{\mathrm{in}},\bar{k}_1}(z_1,z_2,\omega_{\mathrm{in}},\omega_1)$$

$$\equiv (\Delta\omega)^2 \left| \left[\overleftrightarrow{\mathbf{H}}^{\mathrm{LN}}_{\bar{k}_{\mathrm{in}},2\bar{k}_{\mathrm{in}}-\bar{k}_1}(z_2,z_1,\omega_{\mathrm{in}},2\omega_{\mathrm{in}}-\omega_1) \right]_{\xi_2,\xi_1} \right|^2. \tag{71}$$

This expression is invariant for swapping the two observing conditions, and it is also proportional to $I_{\mathrm{in}}{}^{2}$, because an entangled-photon pair is emitted from a biexciton. On the other hand, the second term in Eq. (70) has a finite value for arbitrary pair of ω_1 and ω_2, and represents the accidental coincidence of emitted photons from independent two biexcitons, because this is just the product of two one-photon scattering intensities as

$$C^{(2)\mathrm{N}}_{\xi_1,\xi_2,\bar{k}_{\mathrm{in}},\bar{k}_1,\bar{k}_2}(z_1,z_2,\omega_{\mathrm{in}},\omega_1,\omega_2)$$

$$\equiv C^{(1)}_{\xi_1,\bar{k}_{\mathrm{in}},\bar{k}_1}(z_1,\omega_{\mathrm{in}},\omega_1)C^{(1)}_{\xi_2,\bar{k}_{\mathrm{in}},\bar{k}_2}(z_2,\omega_{\mathrm{in}},\omega_2) \tag{72}$$

This is also invariant for swapping the two observing conditions, and proportional to $I_{\mathrm{in}}{}^{4}$. The third term in Eq. (70) represents the interference between the two observing point, and has a value only for $\omega_1 \simeq \omega_2$. Therefore, we neglect this term in the following discussion.

According to Sec. 3.10 in Ref. 11, we suppose the translational masses of excitons and biexcitons are, respectively, $m_{\mathrm{ex}} = 2.3m_0$ and $m_{\mathrm{bx}} = 2.3m_{\mathrm{ex}}$, where m_0 is the free electron mass. These masses were measured by

RHPS experiments.[11,50,51] However, in our calculation, we do not consider the difference of the mass of longitudinal excitons from that of transverse one. From Sec. 3.2 in Ref. 11, the transverse exciton energy at band edge is $\hbar\omega_T = 3.2022$ eV, LT splitting energy is $\Delta_{LT} = 5.7$ meV, and background dielectric constant of CuCl is $\varepsilon_{bg}^{ex} = 5.59$. Further, according to Sec. 3.7 in Ref. 11, the binding energy of biexciton lowest level is $\Delta_{bx} = 32.2$ meV. The energy of excitons including the center-of-mass kinetic energy is written as

$$\hbar\omega_{\xi,\bar{k},m} = \hbar\omega_T + \frac{\hbar^2}{2m_{ex}}\left(\bar{k}^2 + q_m{}^2\right). \tag{73}$$

The energy of biexciton is

$$\hbar\Omega_{\bar{k},m} = 2\hbar\omega_T - \Delta_{bx} + \frac{\hbar^2}{2m_{bx}}\left(\bar{k}^2 + q_m{}^2\right). \tag{74}$$

We use the other biexciton parameters reported in Ref. 53: The phenomenological damping width is $\gamma_{bx} = \hbar/50$ ps $= 13.2$ μeV, and the effective volume is $|\Phi|^2 = (4000/2) \times (0.541 \text{ nm})^3/4 = 80$ nm^3, where 0.541 nm is the lattice constant of CuCl, and 4000 is a parameter representing the nonlinear strength. In most of all calculations, we consider the exciton nonradiative damping width as $\gamma_{ex} = 0.5$ meV.

Because of the translational symmetry in $x - y$ plane, the in-plane wavenumber of the system is conserved. In the following discussion, we suppose that the pump field is perpendicular to the layers, and biexcitons have zero in-plane wavenumber. Then, a scattered photon with $\bar{k}$ makes a pair with the one having $-\bar{k}$. However, their frequencies are different in general satisfying the energy conservation $\omega_1 + \omega_2 = 2\omega_{in}$. In the present paper, we define the scattering angle θ as $\bar{k} = (\omega_T/c)\sin\theta$, which is approximately equal to the scattering angle in vacuum.

IV. RESULTS

By using the theoretical framework discussed in the previous sections, we calculate the scattering spectra by bulk crystal and by thin film in Sec. IV A. In Sec. IV B, we discuss the difference of entangled photon generation by thin film from that by bulk crystal, and show the thickness dependence of generation efficiency and performance by RHPS in CuCl. Finally, we discuss the the generation from a DBR cavity embedding a CuCl layer in Sec. IV C.

A. Scattering spectra

Fig. 3 shows forward (transmission side) scattering spectra of RHPS from a CuCl film with thickness $d = 7$ μm. We plot $C^{(1)}_{\xi,\bar{k}_{in}=0,\bar{k}=(\omega_T/c)\sin\theta}(z > d, \omega_{in}, \omega)$ as a function of ω for scattering angles $\theta = 0°$, 30°, and 60°,

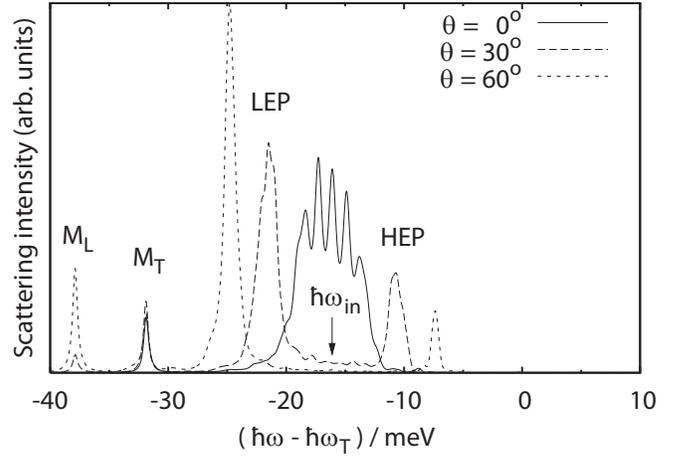FIG. 3: Forward scattering spectra from a CuCl film with thickness $d = 7$ μm. The film exists in vacuum, and the pump beam is perpendicular to it. The pump frequency ω_{in} corresponds to the two-photon absorption due to the biexciton. The results for scattering angles $\theta = 0°$, 30°, and 60° are plotted with different lines as functions of scattering frequency ω.

and the spectra are summed for all the polarization direction $\xi = \{x, y, z\}$. The CuCl film exists in vacuum, and the pump frequency is tuned to the two-photon absorption involving biexcitons as $\hbar\omega_{in} \simeq \hbar\omega_T - \Delta_{bx}/2$. Actually, $\hbar\omega_{in}$ is not exactly $\hbar\omega_T - \Delta_{bx}/2$, because we must also consider the phase-matching condition (wavevector conservation) between two polaritons and a biexciton.[11] Since the shapes of scattering spectra do not depend on the input power I_{in}, we plot the scattering intensity with arbitrary units. The decay paths of biexcitons are depicted in Fig. 1. As seen in Fig. 3, at $\theta = 0°$, we have multiple peaks at $\hbar\omega - \hbar\omega_T \simeq -\Delta_{bx}/2 = -16.1$ meV and a single peak at $\hbar\omega - \hbar\omega_T \simeq -\Delta_{bx} = 32.2$ meV. The latter is called M_T peak, which is emitted by the biexciton relaxation into transverse exciton level (exciton-like polariton).[11] The remaining polariton with frequency $\omega \simeq \omega_T$ propagates backward, but it cannot go outside the film because of the absorption. On the other hand, the multiple peaks at $\hbar\omega - \hbar\omega_T \simeq -16.1$ meV originate from the biexciton relaxation into two polaritons, and the peak structure is due to the interference inside the film with $d = 7$ μm. Increasing the scattering angle, the entangled peaks are split into lower and higher energy sides satisfying the energy and wavevector conservations as discussed in Ref. 37. These peaks are the LEP and HEP, and the intensity of HEP is usually smaller than that of LEP, because of the strong absorption near the bare exciton energy ω_T. The angle dependence of the peak positions obeys the discussion of Ref. 37. The peak at $\hbar\omega - \hbar\omega_T \simeq -\Delta_{bx} - \Delta_{LT}$ is called M_L, which is emitted by the biexciton relaxation into longitudinal exciton state. The emitted photon cannot go outside when $\theta = 0°$ because it is polarized in z direction (longitudinal), and the remaining exciton also cannot go outside due to the
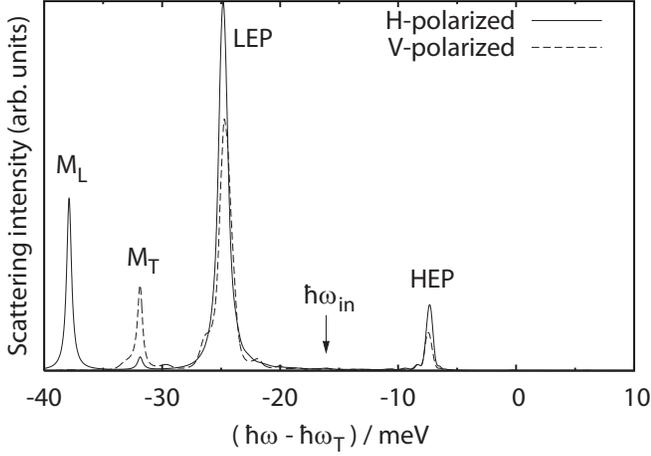
FIG. 4: The scattering spectra of horizontal(H)- and vertical(V)-polarizations are shown. The film thickness is $d = 7$ μm, and the scattering angle is $\theta = 60°$. The other parameters are the same as in Fig. 3.

strong absorption even for $\theta > 0°$.

Fig. 4 shows the polarization-resolved scattering spectra. The film thickness is also $d = 7$ μm and the scattering angle is $\theta = 60°$. H and V represent the horizontal and vertical polarizations, respectively, with respect to the scattering plane. The M_L peak consists of only H-polarized light, because V-polarization does not contain the longitudinal component. Concerning the LEP and HEP peaks, these scattering intensities depend on the polarization. We generally get this behavior at a non-zero scattering angle, because the reflectance at the surface is in general different for the two polarizations. When we resolve the spectra with circular polarizations, the spectra of left- and right-polarizations are the same for any scattering angles and frequencies.

Fig. 5(a) shows the polarization-resolved scattering spectra for thickness $d = 200$ nm. The scattering angle is $\theta = 60°$ and the pump frequency is tuned to excite the $m = 6$ biexciton state. Compared to the spectra for bulk crystal in Fig. 4, there are more than two peaks in the LEP-HEP frequency region. The peak positions are different for H- and V-polarizations, and they do not obey the angle-frequency relation for bulk crystal.[37] The spectral shape can be interpreted by the exciton-photon coupled modes[17,18,21,32,33,35] in the thin film, which have been discussed in relation with the radiative decay of excitons in nano-to-bulk crossover regime.[22–25] Due to the breaking of translational symmetry in z direction, the lower and upper polaritons in bulk material are no longer good eigen states, but instead we obtain the exciton-photon coupled modes with discrete energy levels and radiative decay rates in the case of thin films. A created biexciton spontaneously decays into these coupled modes with emitting a photon conserving the energy and in-plane wavevector. By using the method in Ref. 18, we calculated the exciton-photon coupled modes with V-
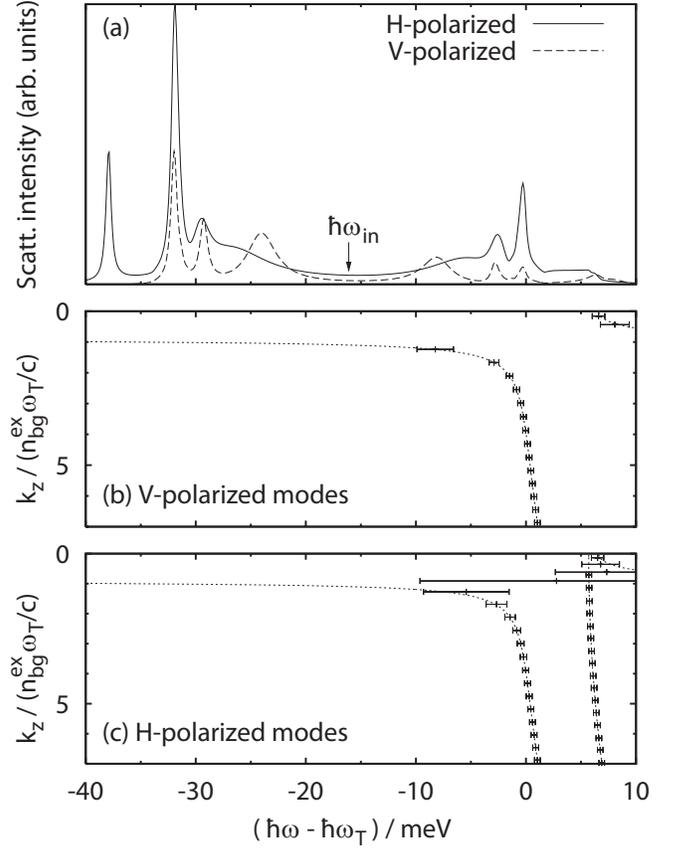

FIG. 5: (a) Polarization-resolved scattering spectra for thickness $d = 200$ nm and scattering angle $\theta = 60°$. The film exists in vacuum and the pump frequency is tuned to resonantly excite the $m = 6$ biexciton state. (b) Dashed lines are the dispersion relation of exciton-polariton in bulk crystal. The horizontal bars represent the exciton-photon coupled modes with V-polarization in the film with $d = 200$ nm. The bar length is the sum of radiative and nonradiative decay rates and the center is the resonance frequency. (c) The H-polarized modes are plotted. Because of the breaking of translational invariance in the z direction and the non-zero scattering angle, the longitudinal excitons are also optically allowed.

polarization in the film with $d = 200$ nm as shown in Fig. 5(b) and the modes with H-polarization are shown in Fig. 5(c). The dashed lines represent the dispersion relation of exciton-polariton in bulk crystal, and the horizontal bars are the coupled modes in the thin film. The length of each bar represents the sum of radiative and nonradiative decay rates, and the center is the resonant frequency. Since the H-polarized modes includes the longitudinal components, there are also the exciton-like modes with longitudinal exciton energy. The higher frequency parts of the scattering spectra in Fig. 5(a) apparently reflect the structure of the coupled modes shown in Figs. 5(b) and (c), and the peaks in lower frequency part appear with satisfying the energy conservation. In this way, the scattering spectra of thin films are completely
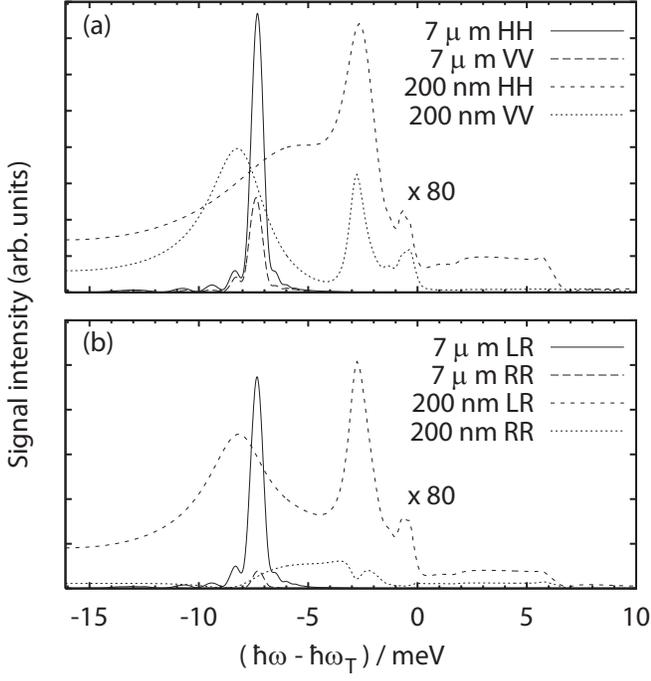
FIG. 6: The two-photon coincidence (signal) intensity is plotted as a function of scattering frequency ω of one photon. The spectra are resolved by the polarization of the two photons. CuCl films with thicknesses $d = 7$ μm and 200 nm are considered, and the scattering angle is $\theta = 60°$. The same pump power is supposed for both the thicknesses. (a) The polarization directions of two photons are resolved in H- and V-axes, and HH and VV pairs are correlated. The pairs with HV and VH polarizations are not generated from the lowest biexciton level in a film. (b) The polarization directions are resolved for circular polarization base. Not only the pairs of left (L) and right (R) circularly polarizations are obtained, but LL and RR pairs are also generated for $\theta > 0$. The spectra of LR and RL are the same, and those of RR and LL are also the same. The spectra of 200 nm are magnified by factor 80 in both (a) and (b). Since the spectra are symmetric about ω_{in}, only the higher frequency side $\omega > \omega_{in}$ is plotted.

different from the bulk one, and they depend on the film thickness, surroundings, and in-plane wavenumber obeying the change of exciton-photon coupled modes as discussed in Ref. 18. Furthermore, in contrast to the spectra for bulk crystal in Fig. 4, the emission near the exciton resonance $\omega \simeq \omega_T$ can go outside the film, because of the large radiative decay rate in the thin film. From these results, the measurement of scattering spectra of RHPS can be considered as a powerful tool[34] to observe the exciton-photon coupled modes in nano-structured materials in addition to the previously performed nonlinear optical responses.[17,33]

B. Entangled-photon generation

Next, we discuss the entangled-photon generation by RHPS process. Fig. 6 shows polarization-resolved spectra of two-photon coincidence measurement. We plot only the signal intensity $C^{(2)S}_{\xi_1,\xi_2,\bar{k}_{in}=0,\bar{k}_1=(\omega_T/c)\sin\theta}(z_1 > d, z_2 > d, \omega_{in}, \omega)$ as a function of scattering frequency ω of one photon (the other photon has a frequency $2\omega_{in}-\omega$). In Fig. 6(a), the pairs with $\xi_1 = \xi_2 = H$ and $\xi_1 = \xi_2 = V$ are considered, and the pairs with different polarizations, such as HV and VH, have no correlation, because the lowest biexciton level with zero angular momentum is excited. Two film thicknesses 7 μm and 200 nm are considered, and the parameters are the same as in Figs. 4 and 5, respectively. In the two calculation, we considered the same pump power I_{in}, and the ratio of signal intensities do not depend on I_{in}. Since the spectra are symmetrical about ω_{in}, we show only the higher energy part $\omega > \omega_{in}$. As similar as the scattering spectra in Fig. 4, the intensities of HH and of VV are not the same in general in the case of non-zero scattering angle. Therefore, the ideal entanglement in Eq. (25b) is not generally obtained, and the entangled state also have RR and LL components, whose spectra are shown in Fig. 6(b). Although this is a general property of bulk crystals, the situation is different in the case of nano-to-bulk crossover regime. As seen in Fig. 6(a), we can obtain the same signal intensities for HH and VV at frequencies $\hbar\omega - \hbar\omega_T = -9.8$ and -7.7 meV for $d = 200$ nm, and the signal intensities of RR and LL become nearly zero at frequency -8.8 meV in Fig. 6(b), while it is slightly different from the peak frequency -8.2 meV of LR spectrum. These results mean that the state of emitted photon pairs can be modified by tuning the film thickness, scattering angle, and scattering frequency in the case of thin films. For example, at frequency -8.8 meV for $d = 200$ nm, we can get the entangled state $(|LR\rangle + |RL\rangle)/\sqrt{2}$, while the proportions of $|HH\rangle$ and $|VV\rangle$ are not equal as seen in Fig. 6(a), because the polarization basis of the two photons are different for $\theta \neq 0$. On the other hand, at frequencies -9.8 and -7.7 meV, we get the entangled pairs with the same HH and VV proportions, while they contains RR and LL components.

Furthermore, even if the scattering angle is $\theta = 0°$, in contrast to the bulk case, the scattering peaks are not at $\omega = \omega_T$ in general in the case of thin films. Therefore, the maximally entangled photon pairs are obtained by the frequency filtering under the observation at $\theta = 0°$. Fig. 7(a) shows the spectrum of signal intensity (generation efficiency) obtained by a CuCl film with thickness $d = 200$ nm for scattering angle $\theta = 0°$. The proportions of HH and VV are the same, and RL and LR paris are not emitted. As seen in Fig. 7(a), the peaks appear not at $\omega = \omega_{in}$ but close to the resonance frequencies of the exciton-photon coupled modes shown in Fig. 7(c) (but not just at the resonance frequency because we get weaker absorption at frequency far from ω_T). In this way,
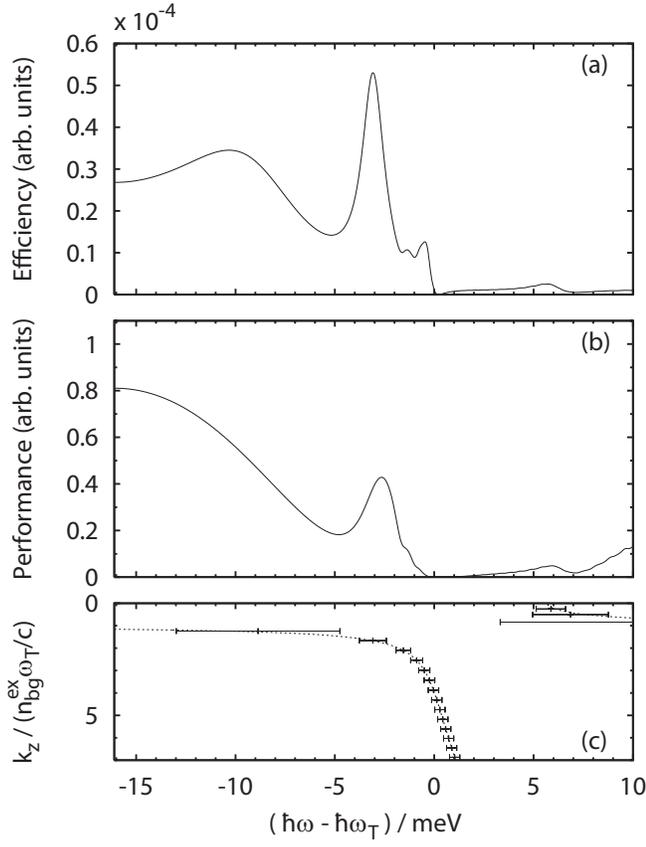
FIG. 7: (a) The generation efficiency (signal intensity) from a CuCl film with thickness $d = 200$ nm is plotted as a function of scattering frequency ω. The biexciton state $m = 6$ is resonantly excited, and the scattering angle is $\theta = 0°$. (b) The spectrum of the corresponding performance P. The generation efficiency and the performance are normalized in the same manner as in Fig. 8. (c) The exciton-photon coupled modes for $\theta = 0°$ in the film are plotted, while $\theta = 60°$ in Fig. 5(b).
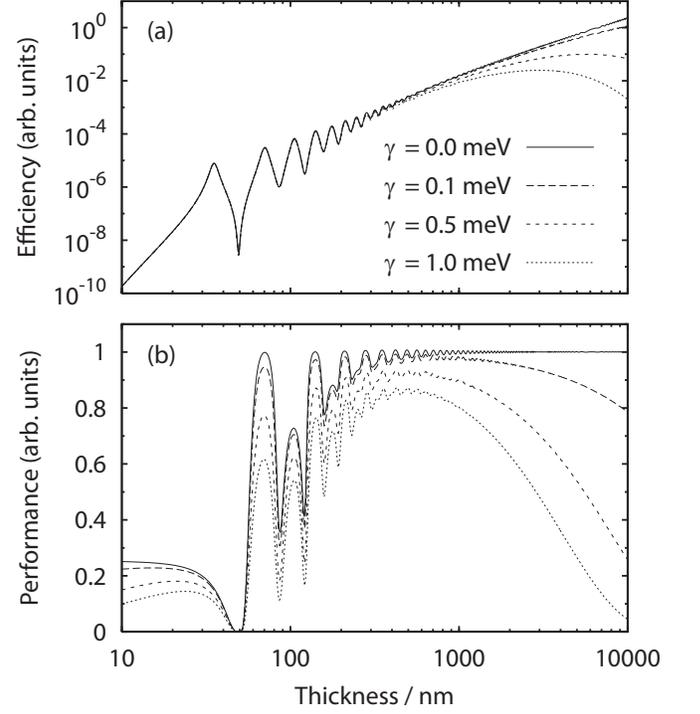

FIG. 8: Thickness dependences of (a) generation efficiency $S/I_{\rm in}^2$ and (b) performance P. The scattering angles are $\theta = 0°$ and the frequencies are $\omega_{1/2} = \omega_{\rm in} \pm 0^+$. To suppress the interference effect, outside medium is the dielectrics with $\varepsilon_{\rm bg}^{\rm ex}$. The results for $\gamma_{\rm ex} = 0$, 0.1, 0.5, and 1.0 meV are plotted with different lines. The performance is normalized to the ideal quantity.

compared to the bulk crystals[10,13] and also to the simple quantum dots,[4,5,7] the nano-to-bulk crossover regime has a variety of degrees of freedom to tune the generated state.

For the high-power generation of the entangled photons, the important factors are the generation efficiency and also the statistical accuracy, i.e., the amount of unentangled pairs. For a pumping beam with power $I_{\rm in}$, the signal intensity $S \propto C^{(2)S}$ (amount of entangled pairs) is proportional to $I_{\rm in}^2$, while the noise intensity $N \propto C^{(2)N}$ (amount of unentangled pairs) is proportional to $I_{\rm in}^4$, because an unentangled pair is involved with two biexcitons. This implies that, by increasing the pump power $I_{\rm in}$, the S/N ratio decreases in contrast to the increase in S.[13] To evaluate the material potential for the generation of strong and qualified entangled-photon beams, we introduce another measure termed "performance" P defined as the signal intensity S under a certain S/N ratio α ($I_{\rm in}$ is tuned to give this ratio). This quantity $P = S^2/\alpha N$

does not depend on $I_{\rm in}$ and reflects the material potential. Fig. 7(b) shows the spectrum of the performance. As comparing with Fig. 7(c), the spectrum of P basically reflects the exciton-photon couples modes. However, since the spectrum of the noise (twice the scattering intensity) is different from the signal one, the Figs. 7(a) and 7(b) are slightly different. The most significant difference is the spectra around $\omega = \omega_{\rm in} \sim \omega_{\rm T} - 16.1$meV. While both S and P mostly reflect the resonance frequency of the exciton-photon coupled modes, the performance is maximized at $\omega = \omega_{\rm in}$, because P is strongly affected by the nonradiative damping, which becomes smaller at that frequency.

Fig. 8 shows the thickness dependences of (a) generation efficiency $S/I_{\rm in}^2$ and (b) performance P. The shapes of P curves do not depend on a chosen α, and the maximum value is normalized to unity. We also plot the generation efficiency with arbitrary units, because the estimation of absolute signal intensities are sensitive to the change of measurement conditions, while the spectral shape and thickness dependence do not depend on such conditions. For simplicity, we assume that the two scattering fields are forward and perpendicular to the film ($\theta = 0°$) and the frequencies are $\omega_{1/2} = \omega_{\rm in} \pm 0^+$. The pump frequency is tuned to the two-photon absorption in

bulk material. The results for nonradiative decay rates $\gamma_{ex} = 0$, 0.1, 0.5, and 1.0 meV are plotted with different lines. In order to suppress the oscillation due to the interference as seen in Fig. 3, we suppose that the CuCl film exists in a dielectric medium with ε_{bg}^{ex}. The results for the film in vacuum will be shown in Fig. 9. In Fig. 8, the oscillating behavior in the nanometer thickness range is due to the biexciton confinement and the modification of the energy structure of exciton-photon coupled modes. The RHPS effectively occurs when the resonance energy of the coupled mode is just equal to half the biexciton energy. The maximum performance shown in Fig. 8(b) is the ideal quantity, and it only depends on measurement conditions, such as resolutions of angle and frequency, but not on material parameters.

As seen in Fig. 8(a) and also in Ref. 12, the optimal thickness for generation efficiency depends on γ_{ex}, and it is on the order of micrometers or more for CuCl crystals. However, as seen in Fig. 8(b), the performance significantly decreases from the ideal value at a thickness of micrometers for nonzero γ_{ex}, because the nonradiative decay easily increases the amount of unentangled pairs. Therefore, when we use bulk crystals, the generation efficiency (generation probability for one pump pulse) is limited by a desired statistical accuracy (S/N ratio).[13] However, at a thickness from 50 to 1000 nm, as expected, a nearly ideal performance can be obtained at particular thicknesses even if γ_{ex} is nonzero. This is because the radiative decay is dominant owing to the exciton superradiance,[17,18] and the entangled pairs can go outside the film without decreasing the amplitude. Therefore, thin films generally show a high performance, and this rapid decay is also desired for the high-repetition excitation, which also recovers the signal intensity while maintaining the S/N ratio.[13]

C. With DBR cavity

Although a good performance is obtained at a thickness of hundreds nanometers, the generation efficiency of such thin films is much lower than that of bulk crystals as seen in Fig. 8(a), and a strong pump power is required to achieve a sufficient signal intensity at such thickness range. While the superradiant excitons maintain the large nonlinearity (excitonic component),[17] this low efficiency simply comes from the small thickness (interaction volume). This problem can be overcome by using an optical cavity in the strong-coupling regime, because we can control both the interaction volume and radiative decay rate using two parameters: quality factor (Q-factor) of cavity and thickness of CuCl. This aspect is different from the simple semiconductor microcavity, in which the interaction volume and radiative decay rate are respectively enhanced in strong- and weak-coupling regimes.

Although a high generation efficiency can be achieved by using a high-Q cavity, we have to simultaneously re-
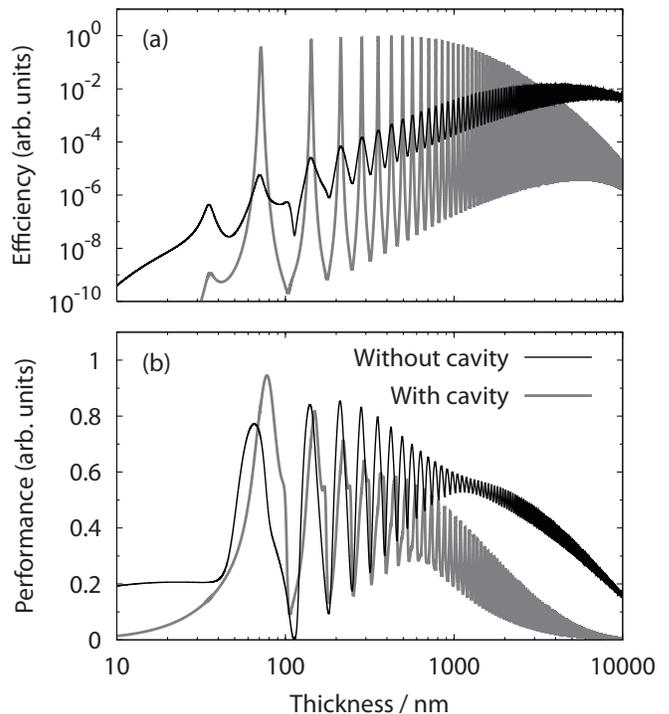

FIG. 9: Thickness dependences of (a) generation efficiency S/I_{in}^2 and (b) performance P. The black lines represent the results for a bare CuCl film existing in vacuum. The scattering frequencies are the same as that of pumping beam, and scattering is forward with $\theta = 0°$. The gray lines represent the results for DBR cavity embedding a CuCl layer shown in Fig. 2(b). The mode frequency of the optical cavity is tuned to ω_T, and the scattering is backward with $\theta = 180°$. In both cases, $\gamma_{ex} = 0.5$ meV. The performance is normalized in the same manner as in Fig. 8.

alize a rapid radiative decay of entangled photons inside the cavity. Therefore, we consider a low-Q cavity as reported in Ref. 69, namely, a CuCl layer in a DBR cavity composed of PbF_2 and $PbBr_2$ as seen in Fig. 2(b). Here, since the translational invariance is broken at the thickness of nanometers, the generated photons can go forward and also backward in contrast to the bulk case. Therefore, we suppose a high reflectance on the transmission side to suppress the leakage of entangled photons, and we focus on the backward emission. The DBR cavity is considered by the background dielectric function $\varepsilon_{bg}(\boldsymbol{r}, \omega)$ in Eq. (9). The refractive indexes of PbF_2 and $PbBr_2$ are 1.86 and 2.95, respectively. The gray lines in Fig. 9 represent the backward emission from the cavity structure, where the cavity mode frequency is tuned to ω_T, $\gamma_{ex} = 0.5$ meV, and the periods of the incident and transmitted sides are 4 and 16, respectively (Q-factor is 50). This system corresponds to the weak bipolariton regime[15,16] (but the strong-coupling regime of excitons and photons), where the energy splitting between polariton and biexciton levels is small compared with their broadening. This situation is in contrast to that in Refs. 15 and 16, where the strong enhancement

of entangled-photon generation from a quantum well in a high-Q cavity has been discussed on the basis of the biexcitonic cavity-QED picture or the strong bipolariton picture. As shown in Fig. 9(a), since biexcitons are effectively created, the generation efficiency is significantly enhanced at a thickness of nanometers, and it is larger than the maximum value in the case of bare CuCl film existing in vacuum (black line). The enhancement also occurs when the polariton energy (exciton-photon coupled mode) is equal to half the biexciton energy, which is consistent with the results in Refs. 15 and 16. Compared with Fig 8(a), the period of the oscillation is doubled, because the RHPS involving biexcitons with odd-parity center-of-mass motion is forbidden in the one-sided optical cavity. On the other hand, as shown in Fig. 9(b), at a thickness of micrometers, the performance is suppressed compared with that of the bare CuCl film. This is because of the multiple reflections inside the cavity, and the scattered fields non-radiatively decay during the propagation. In contrast, at the thickness of nanometers, particularly at 80 nm, the performance almost maintains the ideal quantity. This is due to the enhancement of the radiative decay rate by exciton superradiance, and the enhancement of generation efficiency is simultaneously obtained by the cavity effect in the strong-coupling regime.

Finally, in Figs. 10(a) and (b), we show the spectra of generation efficiency and performance, respectively, in the case of CuCl film with thickness $d = 72$ nm embedded in the DBR cavity discussed above. This thickness is chosen to achieve a high generation efficiency, while the performance at $\omega = \omega_{in}$ is 0.86, which is smaller than the maximum value in Fig. 9(b). However, compared to the thin film without the cavity, the generation efficiency is significantly increased and the high performance is successfully maintained due to the rapid radiative decay. Further, while the pump frequency ω_{in} is assumed to the two-photon absorption frequency in bulk CuCl in Figs. 10(a) and (b), we have numerically checked that, when ω_{in} is correctly tuned to the eigen frequency of a confined biexciton mode, the generation efficiency is enhanced more dramatically with maintaining the high performance in the case with DBR cavity.

In Fig. 10(c), the exciton-photon coupled modes are plotted with horizontal bars, and we can find that one mode with high radiative decay rate exists close to the pump frequency ω_{in} (two-photon absorption frequency of biexcitons). This mode corresponds to the lower cavity polariton, and the strong electric field in the cavity enhances the generation efficiency of biexcitons due to the cavity-induced double resonance.[70] Furthermore, the generated entangled excitons rapidly decay into photons through this polariton mode, which ensures the high performance at the same time.

In this way, by using an optical cavity embedding a CuCl layer with a thickness of nanometers, we can obtain high efficiency and performance simultaneously. To avoid the leakage of generated photons, the reflectance on the
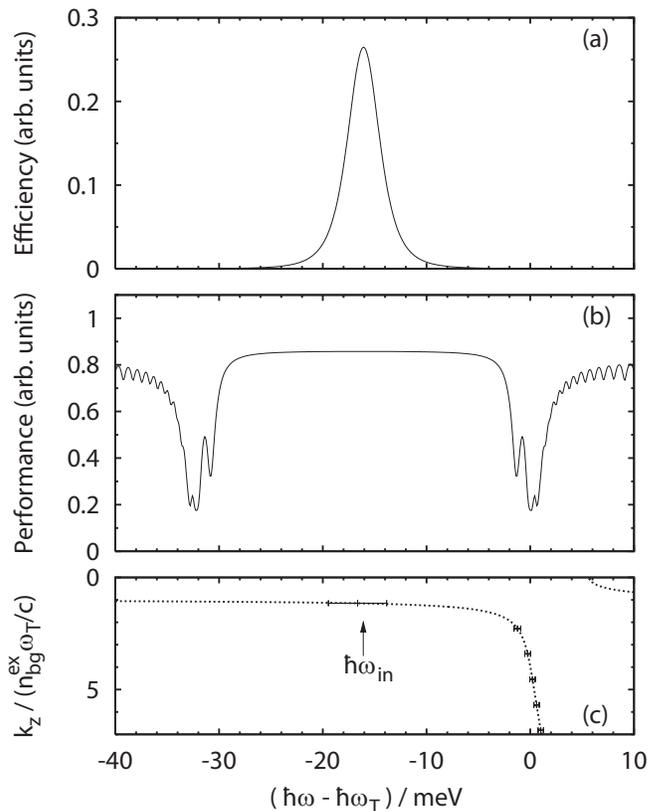

FIG. 10: (a) The generation efficiency (signal intensity) is plotted as a function of scattering frequency ω. A CuCl film with thickness $d = 72$ nm is embedded in the DBR cavity considered in Fig. 9, and the other parameters are also the same. (b) The spectrum of the corresponding performance P. (c) The exciton-photon coupled modes in the film are plotted in the same manner as in Fig. 5(b).

transmission side should be high enough, but that on the incident side should not be high to obtain a rapid radiative decay rate. Once we choose a cavity structure, we can numerically determine the optimal thickness of CuCl layer, in which an exciton-photon coupled mode has half the biexciton frequency, a rapid radiative decay rate, and also large exciton component (large nonlinearity) to achieve high performance and generation efficiency. Such a coupled mode is an unique feature in the nano-to-bulk crossover regime.

V. SUMMARY

We have developed a theoretical framework for the investigation of the biexciton-involved RHPS based on the QED theory for excitons.[44] Compared to the previous theories,[12,39] our method can be applied to nano-to-bulk crossover regime because we explicitly consider the center-of-mass motion of exciton. Further, we can discuss the polarization correlation of entangled pairs and the surroundings of the excitonic layer, such as the DBR

cavity structure. While we considered CuCl films in actual calculation, by treating several relative exciton levels and by correctly calculating the center-of-mass wave-functions of excitons confined in finite crystal including the effect of dead layer,[71] our theoretical framework can be applied to other materials in principle. Further, by correctly treat the modification of relative motion of excitons and biexcitons strongly confined in nano crystals and also the Pauli's exclusion principle, our framework can be extended for the investigation of single quantum dot, the deterministic generation of entangled photons.

We have calculated the scattering spectra of RHPS from CuCl films with bulk-like and submicron thicknesses. For the bulk-like thickness, the four peaks called M_T, M_L, LEP and HEP are reproduced. On the other hand, the scattering spectra of the thin film are significantly modified from the bulk ones, and we found that they reflect the exciton-photon coupled modes in the thin film.[17,18,21,33,35] Therefore, the RHPS measurement is also useful to observe the exciton-photon coupled modes in nano-structured materials[34] as well as the four-wave mixing[17,29,35] and the two-photon excitation scattering.[33] We also found that semiconductor thin films have much degrees of freedom to control generated states of entangled photon pairs.

In addition to the signal intensity of entangled-photon generation, we also discuss the performance of the material structure by considering the noise intensity from independent two biexcitons. Although the thickness dependence of signal intensity has a maximum value at particular thickness determined by nonradiative decay rate of excitons,[12,39] a high performance is generally obtained at thickness of nanometers due to the rapid radiative decay of excitons. However, the generation efficiency of such thin films is much weaker compared to the bulk one. We have demonstrated that, by using a DBR cavity embedding an excitonic layer in the nano-to-bulk crossover regime, the generation efficiency can be enhanced while maintaining the high performance.

For the pursuit of high-power and high-quality but probabilistic generation of entangled photons, which is essential for the next-generation technologies of fabrication and chemical reaction,[9] the biexciton-involved RHPS shows a quite high generation efficiency compared to that of PDC method. From the viewpoint of the quality of generated entangled pairs, the RHPS method can show a high performance and a high generation efficiency simultaneously by using and an optical cavity embedding a CuCl nano-layer. Further, it has much degrees of freedom to control the generated states of entangled photons. We believe that our results make a breakthrough in high-power and high-quality entangled-photon generation.

* Present address: Laboratoire Matériaux et Phénomènes Quantiques, Université Paris Diderot-Paris 7 et CNRS, Case 7021, Bâtiment Condorcet, 75013 Paris, France. E-mail: motoaki.bamba@univ-paris-diderot.fr

[1] A. Einstein, B. Podolsky, and N. Rosen, Phys. Rev. 47, 777 (1935).

[2] P. G. Kwiat, K. Mattle, H. Weinfurter, A. Zeilinger, A. V. Sergienko, and Y. Shih, Phys. Rev. Lett. 75, 4337 (1995).

[3] P. G. Kwiat, E. Waks, A. G. White, I. Appelbaum, and P. H. Eberhard, Phys. Rev. A 60, R773 (1999).

[4] N. Akopian, N. H. Lindner, E. Poem, Y. Berlatzky, J. Avron, D. Gershoni, B. D. Gerardot, and P. M. Petroff, Phys. Rev. Lett. 96, 130501 (2006).

[5] R. M. Stevenson, R. J. Young, P. Atkinson, K. Cooper, D. A. Ritchie, and A. J. Shields, Nature 439, 179 (2006).

[6] R. J. Young, R. M. Stevenson, A. J. Hudson, C. A. Nicoll, D. A. Ritchie, and A. J. Shields, Phys. Rev. Lett. 102, 030406 (2009).

[7] C. L. Salter, R. M. Stevenson, I. Farrer, C. A. Nicoll, D. A. Ritchie, and A. J. Shields, Nature 465, 594 (2010).

[8] A. Dousse, J. Suffczynski, A. Beveratos, O. Krebs, A. Lemaitre, I. Sagnes, J. Bloch, P. Voisin, and P. Senellart, Nature 466, 217 (2010).

[9] Y. Kawabe, H. Fujiwara, R. Okamoto, K. Sasaki, and S. Takeuchi, Opt. Express 15, 14244 (2007).

[10] K. Edamatsu, G. Oohata, R. Shimizu, and T. Itoh, Nature 431, 167 (2004).

[11] M. Ueta, H. Kanzaki, K. Kobayashi, Y. Toyozawa, and E. Hanamura, Excitonic Processes in Solids (Springer-Verlag, Berlin, 1986).

[12] S. Savasta, G. Martino, and R. Girlanda, Solid State Commun. 111, 495 (1999).

[13] G. Oohata, R. Shimizu, and K. Edamatsu, Phys. Rev. Lett. 98, 140503 (2007).

[14] M. Bamba and H. Ishihara, Phys. Rev. Lett. 105, 123906 (2010).

[15] H. Ajiki and H. Ishihara, J. Phys. Soc. Jpn. 76, 053401 (2007).

[16] H. Oka and H. Ishihara, Phys. Rev. Lett. 100, 170505 (2008).

[17] M. Ichimiya, M. Ashida, H. Yasuda, H. Ishihara, and T. Itoh, Phys. Rev. Lett. 103, 257401 (2009).

[18] M. Bamba and H. Ishihara, Phys. Rev. B 80, 125319 (2009).

[19] A. Tredicucci, Y. Chen, F. Bassani, J. Massies, C. Deparis, and G. Neu, Phys. Rev. B 47, 10348 (1993).

[20] Z. K. Tang, A. Yanase, Y. Segawa, N. Matsuura, and K. Cho, Phys. Rev. B 52, 2640 (1995).

[21] M. Bamba and H. Ishihara, J. Phys. Soc. Jpn. **78**, 043701 (2009).

[22] J. Knoester, Phys. Rev. Lett. **68**, 654 (1992).

[23] G. Björk, S. Pau, J. M. Jacobson, H. Cao, and Y. Yamamoto, Phys. Rev. B **52**, 17310 (1995).

[24] V. M. Agranovich, D. M. Basko, and O. A. Dubovsky, J. Chem. Phys. **106**, 3896 (1997).

[25] H. Ajiki, J. Lumin. **94-95**, 173 (2001).

[26] H. Ishihara and K. Cho, Phys. Rev. B **53**, 15823 (1996).

[27] K. Akiyama, N. Tomita, Y. Nomura, and T. Isu, Appl. Phys. Lett. **75**, 475 (1999).

[28] H. Ishihara, T. Amakata, and K. Cho, Phys. Rev. B **65**, 035305 (2001).

[29] H. Ishihara, K. Cho, K. Akiyama, N. Tomita, Y. Nomura, and T. Isu, Phys. Rev. Lett. **89**, 017402 (2002).

[30] K. Cho, *Optical Response of Nanostructures: Microscopic Nonlocal Theory* (Springer-Verlag, Berlin, 2003).

[31] H. Ishihara, Phys. Rev. B **67**, 113302 (2003).

[32] H. Ishihara, J. Kishimoto, and K. Sugihara, J. Lumin. **108**, 343 (2004).

[33] A. Syouji, B. P. Zhang, Y. Segawa, J. Kishimoto, H. Ishihara, and K. Cho, Phys. Rev. Lett. **92**, 257401 (2004).

[34] H. Ishihara, A. Syouji, Y. Segawa, and M. Bamba, J. Phys.: Condens. Matter **19**, 445008 (2007).

[35] O. Kojima, T. Isu, J. Ishi-Hayase, A. Kanno, R. Katouf, M. Sasaki, and M. Tsuchiya, J. Phys. Soc. Jpn. **77**, 044701 (2008).

[36] H. Yasuda and H. Ishihara, Phys. Rev. B **79**, 193308 (2009).

[37] M. Inoue and E. Hanamura, J. Phys. Soc. Jpn. **41**, 1273 (1976).

[38] E. Hanamura and T. Takagahara, J. Phys. Soc. Jpn. **47**, 410 (1979).

[39] S. Savasta and R. Girlanda, Phys. Rev. B **59**, 15409 (1999).

[40] B. Huttner and S. M. Barnett, Phys. Rev. A **46**, 4306 (1992).

[41] L. Knöll, S. Scheel, and D.-G. Welsch, *QED in Dispersing and Absorbing Dielectric Media*, in *Coherence and Statistics of Photons and Atoms*, edited by J. Peřina, (Wiley, New York, 2001), chapter 1, pp. 1–64.

[42] T. Östreich, K. Schonhammer, and L. J. Sham, Phys. Rev. Lett. **74**, 4698 (1995).

[43] T. Östreich, K. Schonhammer, and L. J. Sham, Phys. Rev. B **58**, 12920 (1998).

[44] M. Bamba and H. Ishihara, Phys. Rev. B **78**, 085109 (2008).

[45] K. Cho, Prog. Theor. Phys. Suppl. **106**, 225 (1991).

[46] K. Cho, J. Phys. Soc. Jpn. **55**, 4113 (1986).

[47] T. Itoh, T. Suzuki, and M. Ueta, J. Phys. Soc. Jpn. **42**, 1069 (1977).

[48] T. Itoh and T. Suzuki, J. Phys. Soc. Jpn. **45**, 1939 (1978).

[49] M. Ueta, T. Mita, and T. Itoh, Solid State Commun. **32**, 43 (1979).

[50] T. Mita, K. Sôtome, and M. Ueta, J. Phys. Soc. Jpn. **48**, 496 (1980).

[51] T. Mita, K. Sôtome, and M. Ueta, Solid State Commun. **33**, 1135 (1980).

[52] Y. Nozue, J. Phys. Soc. Jpn. **51**, 1840 (1982).

[53] H. Akiyama, T. Kuga, M. Matsuoka, and M. Kuwata-Gonokami, Phys. Rev. B **42**, 5621 (1990).

[54] E. Tokunaga, A. L. Ivanov, S. V. Nair, and Y. Masumoto, Phys. Rev. B **59**, R7837 (1999).

[55] A. L. Ivanov and H. Haug, Phys. Rev. B **48**, 1490 (1993).

[56] A. L. Ivanov, H. Haug, and L. V. Keldysh, Phys. Rep. **296**, 237 (1998).

[57] E. Tokunaga, A. L. Ivanov, S. V. Nair, and Y. Masumoto, J. Lumin. **87-89**, 216 (2000).

[58] E. Tokunaga, K. Kurihara, M. Baba, Y. Masumoto, and M. Matsuoka, Phys. Rev. B **64**, 045209 (2001).

[59] R. Matloob, R. Loudon, S. M. Barnett, and J. Jeffers, Phys. Rev. A **52**, 4823 (1995).

[60] S. Savasta and R. Girlanda, Phys. Rev. A **53**, 2716 (1996).

[61] T. Gruner and D.-G. Welsch, Phys. Rev. A **54**, 1661 (1996).

[62] S. Savasta, O. D. Stefano, and R. Girlanda, J. Opt. Soc. Am. B **19**, 304 (2002).

[63] M. Khanbekyan, L. Knöll, and D.-G. Welsch, Phys. Rev. A **67**, 063812 (2003).

[64] L. G. Suttorp and M. Wubs, Phys. Rev. A **70**, 013816 (2004).

[65] J. Singh, Phys. Solid State **40**, 728 (1998).

[66] N. Matsuura and K. Cho, J. Phys. Soc. Jpn. **64**, 651 (1995).

[67] W. C. Chew, *Waves and Fields in Inhomogeneous Media* (IEEE, New York, 1995).

[68] A. A. Abrikosov, L. P. Gorkov, and I. E. Dzyaloshinski, *Methods of Quantum Field Theory in Statistical Physics*, (Dover, New York, 1975), chapter 6.

[69] G. Oohata, T. Nishioka, D. Kim, H. Ishihara, and M. Nakayama, Phys. Rev. B **78**, 233304 (2008).

[70] H. Ishihara and K. Cho, Appl. Phys. Lett. **71**, 3036 (1997).

[71] V. M. Agranovich and V. L. Ginzburg, *Crystal Optics with Spatial Dispersion, and Excitons* (Springer-Verlag, Berlin, 1984).